Supporting Information for

Enantiomers of tetrahedral metal-organic cages: a new class of highly efficient G-quadruplex ligands with potential anticancer activities

Sai-Fei Xi,[a] Ling-Yu Bao,[a] Jian-Guo Lin,[b] Qing-Zhu Liu,[b] Ling Qiu,[b] Feng-Li Zhang,[a] Yu-Xia Wang,[a] Zheng-Dong Ding,[a] Ke Li,[b] and Zhi-Guo Gu[a]*

[a] *The Key Laboratory of Food Colloids and Biotechnology, Ministry of Education, School of Chemical and Material Engineering, Jiangnan University, Wuxi 214122, P.R. China*
[b] *Key Laboratory of Nuclear Medicine, Ministry of Health, Jiangsu Key Laboratory of Molecular Nuclear Medicine, Jiangsu Institute of Nuclear Medicine, Wuxi 214063, China*

E-mail: zhiguogu@jiangnan.edu.cn

Table of contents

1. Materials and methods

The human telomeric sequence 5'-AGGGTTAGGGTTAGGGTTAGGG-3' (HTG22), 5'-FAM-AGGGTTAGGGTTAGGGTTAGGG-TAMRA-3' (F22T), of which the donor fluorophore FAM is 6-carboxy-fluorescein and the acceptor fluorophore TAMRA is 6-carboxytetrame-thylrhodamine were synthesized by Sangon Biotechnology (Shanghai, China), and were used without further purification. HTG22 and F22T were dissolved in different buffers (Na^+ buffer: 100 mM NaCl, 10 mM Tris-HCl, pH = 7.4; K^+ buffer: 100 mM KCl, 10 mM Tris-HCl, pH = 7.4), and annealed at 95°C for 5 min and then slowly cooled to room temperature. Concentrations of HTG22 and F22T were determined by measuring the absorbance at 260 nm after melting. The solutions were stored at 4 °C and used after no more than 4 days. The human cancer cell lines MCF-7 (human breast adenocarcinoma), HCT116 (colon carcinoma) and HepG2 (liver carcinoma) were obtained from the Cell Bank of Chinese Academy of Sciences, (Shanghai, China). The reagent 3-[4,5-dimethyl-2-thiazolyl]-2,5-diphenyl-2-tetrazolium bromide (MTT) used for cell lysis was purchased from Sigma (St. Louis, MO, USA). Dulbecco's modified eagle medium (DMEM) and Roswell Park Memorial Institute (RPMI-1640) medium were purchased from Gibco Company (USA). Ultrapure water (18.2 MΩ.cm) was used in all experiments. All other reagents employed were of analytical reagent grade or with highest quality, and purchased from commercial sources and used without further purification. Cages ***R*-1**/***S*-1** and ***R*-2**/***S*-2** were soluble in water, and a stock solution of 1 mM was prepared in water. The stock solution of cages ***R*-3**/***S*-3** and ***R*-4**/***S*-4** were dissolved to 1 mM in DMSO. Further dilution was made in the corresponding buffer according to the required concentrations for all the experiments.

Element analyses were conducted on elementar corporation vario ELIII analyzer. Infrared spectra were measured on an ABB Bomem FTLA 2000-104 spectrometer with KBr pellets in the 400-4000 cm^{-1} region. UV-vis absorbance spectra were collected on Shimadzu UV-2101 PC scanning spectrophotometer. The electrospray ionization mass spectrometry (ESI-MS) spectra were recorded using an LCQ fleet APT/SSQ-710 ESI-

MS spectrometer (Finnigan MAT). Circular dichroism (CD) spectra were carried out using a MOS-450/AF-CD spectro polarimeter at room temperature, which were calibrated conventionally using 0.060% ACS for intensity and a holmium filter for wavelength.

2. Synthesis

1,8-di(imidazole-2-carboxaldehyde)octane was prepared and characterized according to the literatures.[1]

Caution: The perchlorate salt was potentially explosive. Thus, this starting material should be handled in small quantities and with great caution.

General procedure for $[Ni_4L^1_6]Cl_8$ cages (*R*-1 and *S*-1)

(*R*)-1-phenylethylamine (48.5 mg, 0.4 mmol) and 1,8-di(imidazole-2-carboxaldehyde)octane (60.5 mg, 0.2 mmol) were dissolved in 20 mL acetonitrile and heated to reflux for 2 h at 80 °C. After cooling to ambient temperature, solution of $NiCl_2{\cdot}6H_2O$ (31.6 mg, 0.133 mmol) in 10 mL acetonitrile was added with drops and stirred vigorously for 1 h. The resulting solution was cooled and filtered. Crystalline solid of ***R*-1** ($\Lambda\Lambda\Lambda\Lambda$-$[Ni_4(R\text{-}L^1)_6]Cl_8$) was obtained by slow diffusion of diethyl ether into the resulting solution for 1 week. ***S*-1** ($\Delta\Delta\Delta\Delta$-$[Ni_4(S\text{-}L^1)_6]Cl_8$) was prepared following a similar procedure except that (*S*)-1-phenylethylamine instead of (*R*)-1-phenylethylamine was used.

***R*-1**: light purple crystals (48%). IR (KBr cm^{-1}): ν = 3060 (w), 2930 (m), 2850 (w), 1614 (s), 1496 (s), 1442 (s), 1380 (w), 1304 (w), 1085 (m), 1009 (w), 968 (w), 913 (w), 851 (w), 762 (m), 700 (m), 620 (w); ESI-MS (m/z): 474.63 $[Ni_4(L^1)_6Cl]^{7+}$, 559.65 $[Ni_4(L^1)_6Cl_2]^{6+}$, 678.67 $[Ni_4(L^1)_6Cl_3]^{5+}$; Anal. Calcd (%) for $Ni_4C_{192}N_{36}H_{240}Cl_8$: C 64.58, H 6.77, N 14.12, Found: C 64.47, H 6.63, N 14.07. ***S*-1**: light purple crystals (41%). IR (KBr cm^{-1}): ν = 3059 (w), 2930 (m), 2850 (w), 1614 (s), 1497 (s), 1442 (s), 1380 (w), 1304 (w), 1085 (m), 1009 (w), 968 (w), 913 (w), 851 (w), 762 (m), 700 (m), 621 (w); ESI-MS (m/z): 474.63 $[Ni_4(L^1)_6Cl]^{7+}$, 559.65 $[Ni_4(L^1)_6Cl_2]^{6+}$, 678.67 $[Ni_4(L^1)_6Cl_3]^{5+}$;

Anal. Calcd (%) for $Ni_4C_{192}N_{36}H_{240}Cl_8$: C 64.58, H 6.77, N 14.12, Found: C 64.65, H 6.59, N 14.01.

General procedure for $[Ni_4L^1_6][ClO_4]_8$ cages

Crystals of *ΛΛΛΛ*-$[Ni_4(R\text{-}L^1)_6][ClO_4]_8$ and *ΔΔΔΔ*-$[Ni_4(S\text{-}L^1)_6][ClO_4]_8$ were prepared by similar procedure to that of $[Ni_4L^1_6]Cl_8$ cages where $Ni(ClO_4)_2{\cdot}6H_2O$ (31.7 mg, 0.133 mmol) substituted for $NiCl_2{\cdot}6H_2O$.

ΛΛΛΛ-$[Ni_4(R\text{-}L^1)_6][ClO_4]_8$: light purple crystals (54%). IR (KBr cm^{-1}): ν = 3130 (w), 2930 (m), 2858 (w), 1619 (m), 1493 (m), 1448 (s), 1377 (w), 1306 (w), 1090 (s), 918 (w), 847 (w), 763 (m), 703 (m), 620 (w); ESI-MS (m/z): 580.98 $[Ni_4(L^1)_6(ClO_4)_2]^{6+}$, 717.06 $[Ni_4(L^1)_6(ClO_4)_3]^{5+}$, 921.19 $[Ni_4(L^1)_6(ClO_4)_4]^{4+}$; Anal. Calcd (%) for $Ni_4C_{192}N_{36}O_{32}H_{240}Cl_8$: C 56.48, H 5.92, N 12.35, Found: C 56.35, H 5.86, N 12.21. *ΔΔΔΔ*-$[Ni_4(S\text{-}L^1)_6][ClO_4]_8$: light purple crystals (49%). IR (KBr cm^{-1}): ν = 3129 (w), 2930 (m), 2859 (w), 1620 (m), 1491 (m), 1448 (s), 1377 (w), 1306 (w), 1088 (s), 918 (w), 847 (w), 763 (m), 705 (m), 619 (w); ESI-MS (m/z): 580.98 $[Ni_4(L^1)_6(ClO_4)_2]^{6+}$, 717.06 $[Ni_4(L^1)_6(ClO_4)_3]^{5+}$, 921.19 $[Ni_4(L^1)_6(ClO_4)_4]^{4+}$; Anal. Calcd (%) for $Ni_4C_{192}N_{36}O_{32}H_{240}Cl_8$: C 56.48, H 5.92, N 12.35, Found: C 56.33, H 5.79, N 12.26.

General procedure for $[Ni_4L^2_6]Cl_8$ cages (*R*-2 and *S*-2)

***R*-2** and ***S*-2** were synthesised using the procedure described for ***R*-1** and ***S*-1**, substituting (*R*)-1-(4-methoxyphenyl)ethylamine or (*S*)-1-(4-methoxyphenyl)ethylamine for (*R*)-1-phenylethylamine or (*S*)-1-phenylethylamine.

***R*-2**: light purple crystals (51%). IR (KBr cm^{-1}): ν = 3084 (w), 2932 (m), 2850 (w), 1610 (s), 1513 (s), 1445 (m), 1378 (w), 1304 (m), 1243 (s) 1177 (s), 1089 (m), 1022 (m), 962 (w), 915 (w), 827 (m), 762 (m), 606 (w), 538 (w); ESI-MS (m/z): 526.10 $[Ni_4(L^2)_6Cl]^{7+}$, 619.70 $[Ni_4(L^2)_6Cl_2]^{6+}$, 750.73 $[Ni_4(L^2)_6Cl_3]^{5+}$; Anal. Calcd (%) for $Ni_4C_{204}N_{36}O_{12}H_{264}Cl_8$: C 62.33, H 6.77, N 12.83, Found: C 62.14, H 6.59, N 12.68. ***S*-2**: light purple crystals (43%). IR (KBr cm^{-1}): ν = 3084 (w), 2932 (m), 2851 (w), 1610 (s), 1513 (s), 1445 (m), 1380 (w), 1305 (m), 1243 (s), 1179 (s), 1089 (m), 1023 (m), 964 (w),

915 (w), 829 (m), 762 (m), 608 (w), 538 (w); ESI-MS (m/z): 526.10 $[Ni_4(L^2)_6Cl]^{7+}$, 619.70 $[Ni_4(L^2)_6Cl_2]^{6+}$, 750.73 $[Ni_4(L^2)_6Cl_3]^{5+}$; Anal. Calcd (%) for $Ni_4C_{204}N_{36}O_{12}H_{264}Cl_8$: C 62.33, H 6.77, N 12.83, Found: C 62.10, H 6.58, N 12.62.

General procedure for *ΔΔΔΔ*-$[Ni_4(S\text{-}L^2)_6][BF_4]_8$ cage

Light purple crystals of *ΔΔΔΔ*-$[Ni_4(S\text{-}L^2)_6][BF_4]_8$ were prepared by similar procedure to that of *ΔΔΔΔ*-$[Ni_4(S\text{-}L^2)_6]Cl_8$ (***R*-2**) where $Ni(BF_4)_2{\cdot}6H_2O$ (45.3 mg, 0.133 mmol) substituted for $NiCl_2{\cdot}6H_2O$.

ΔΔΔΔ-$[Ni_4(S\text{-}L^2)_6][BF_4]_8$: light purple crystals (44%). IR (KBr cm^{-1}): ν = 3128 (w), 2932 (m), 2857 (w), 1614 (m), 1510 (m), 1447 (s), 1380 (w), 1249 (m), 1179 (w), 1080 (w), 1038 (w), 839 (w), 783 (w), 615 (w); ESI-MS (m/z): 636.82 $[Ni_4(L^2)_6(BF_4)_2]^{6+}$, 781.54 $[Ni_4(L^2)_6(BF_4)_3]^{5+}$, 998.63 $[Ni_4(L^2)_6(BF_4)_4]^{4+}$; Anal. Calcd (%) for $Ni_4C_{204}N_{36}O_{12}H_{264}B_8F_{32}$: C 56.43, H 6.13, N 11.61, Found: C 56.32, H 6.02, N 11.54.

General procedure for $[Ni_4L^3_6]Cl_8$ cages (*R*-3 and *S*-3)

***R*-3** and ***S*-3** were synthesised using the procedure described for ***R*-2** and ***S*-2**, substituting (*R*)-1-(1-naphthyl)ethylamine or (*S*)-1-(1-naphthyl)ethylamine for (*R*) -1-(4-methoxyphenyl)ethylamine or (*S*)-1-(4-methoxyphenyl)ethylamine.

***R*-3**: light purple crystals (40%). IR (KBr cm^{-1}): ν = 3056 (w), 2934 (m), 2852 (w), 1617 (s), 1501 (s), 1446 (s), 1385 (w), 1314 (w), 1175 (w), 1097 (m), 1001 (w), 914 (w), 864 (w), 792 (s), 729 (w), 579 (w); ESI-MS (m/z): 560.45 $[Ni_4(L^3)_6Cl]^{7+}$, 798.81 $[Ni_4(L^3)_6Cl_3]^{5+}$, 1007.37 $[Ni_4(L^3)_6Cl_4]^{4+}$; Anal. Calcd (%) for $Ni_4C_{240}N_{36}H_{264}Cl_8$: C 69.10, H 6.38, N 12.09, Found: C 69.01, H 6.29, N 12.15. ***S*-3**: light purple crystals (37%). IR (KBr cm^{-1}): ν = 3051 (w), 2930 (m), 2853 (w), 1617 (s), 1500 (m), 1445 (s), 1385 (w), 1314 (m), 1175 (s), 1098 (m), 1001 (w), 915 (w), 864 (w), 791 (m), 729 (w), 580(w); ESI-MS (m/z): 560.45 $[Ni_4(L^3)_6Cl]^{7+}$, 798.81 $[Ni_4(L^3)_6Cl_3]^{5+}$, 1007.37 $[Ni_4(L^3)_6Cl_4]^{4+}$; Anal. Calcd (%) for $Ni_4C_{240}N_{36}H_{264}Cl_8$: C 69.10, H 6.38, N 12.09, Found: C 69.03, H 6.31, N 12.00.

General procedure for $[Ni_4L^4_6]Cl_8$ cages (*R*-4 and *S*-4)

***R*-4** and ***S*-4** were synthesised using the procedure described for ***R*-2** and ***S*-2**, substituting (*R*)-1-(2-naphthyl)ethylamine or (*S*)-1-(2-naphthyl)ethylamine for (*R*) -1-(4-methoxyphenyl)ethylamine or (*S*)-1-(4-methoxyphenyl)ethylamine**.**

***R*-4**: colorless crystals (38%). IR (KBr cm^{-1}): ν = 3056 (w), 2930 (m), 2857 (w), 1616 (s), 1491 (s), 1446 (s), 1383 (w), 1310 (m), 1131 (w), 1092 (m), 976 (w), 923 (w), 868 (w), 826 (m), 753 (s), 725 (w), 662 (w); ESI-MS (m/z): 560.45 $[Ni_4(L^4)_6Cl]^{7+}$, 659.76 $[Ni_4(L^4)_6Cl_2]^{6+}$, 798.81 $[Ni_4(L^4)_6Cl_3]^{5+}$; Anal. Calcd (%) for $Ni_4C_{240}N_{36}H_{264}Cl_8$: C 69.10, H 6.38, N 12.09, Found: C 69.29, H 6.27, N 12.18. ***S*-4**: colorless crystals (36%). IR (KBr cm^{-1}): ν = 3056 (w), 2930 (w), 2855 (w), 1617 (s), 1492 (s), 1446 (s), 1383 (w), 1310 (m), 1131 (w), 1092 (m), 975 (w), 923 (w), 868 (w), 825 (m), 753 (s), 725 (w), 662 (w); ESI-MS (m/z): 560.45 $[Ni_4(L^4)_6Cl]^{7+}$, 659.76 $[Ni_4(L^4)_6Cl_2]^{6+}$, 798.81 $[Ni_4(L^4)_6Cl_3]^{5+}$; Anal. Calcd (%) for $Ni_4C_{240}N_{36}H_{264}Cl_8$: C 69.10, H 6.38, N 12.09, Found: C 69.18, H 6.26, N 12.15.

General procedure for *ΛΛΛΛ*-$[Ni_4(R\text{-}L^4)_6][SO_3CF_3]_8$ cage

Colorless crystals of *ΛΛΛΛ*-$[Ni_4(R\text{-}L^4)_6][SO_3CF_3]_8$ were prepared by similar procedure to that of *ΛΛΛΛ*-$[Ni_4(R\text{-}L^4)_6]Cl_8$ (***R*-4**) where $Ni(SO_3CF_3)_2{\cdot}6H_2O$ (47.5 mg, 0.133 mmol) substituted for $NiCl_2{\cdot}6H_2O$.

ΛΛΛΛ-$[Ni_4(R\text{-}L^4)_6][SO_3CF_3]_8$: colorless crystals (37%). IR (KBr cm^{-1}): ν = 3123 (w), 2932 (m), 2859 (w), 1619 (m), 1492 (m), 1447 (m), 1378 (w), 1268 (s), 1156 (m), 1091 (w), 1030 (s), 969 (m), 920 (m), 866 (w), 825 (w), 755 (m), 637 (s); ESI-MS (m/z): 697.64 $[Ni_4(L^4)_6(SO_3CF_3)_2]^{6+}$, 866.98 $[Ni_4(L^4)_6(SO_3CF_3)_3]^{5+}$, 1120.99 $[Ni_4(L^4)_6(SO_3CF_3)_4]^{4+}$; Anal. Calcd (%) for $Ni_4C_{248}N_{36}O_{24}H_{264}S_8F_{24}$: C 58.63, H 5.24, N 9.92, Found: C 58.58, H 5.19, N 9.97.

3. Circular dichroism spectra of tetrahedral cages

Measurements were collected using a 1 cm path-length quartz cuvette. The parameters used were; bandwidth 1 nm, response time 1 sec, wavelength scan range 200-450 nm. For each cage, three scans were accumulated and automatically averaged.

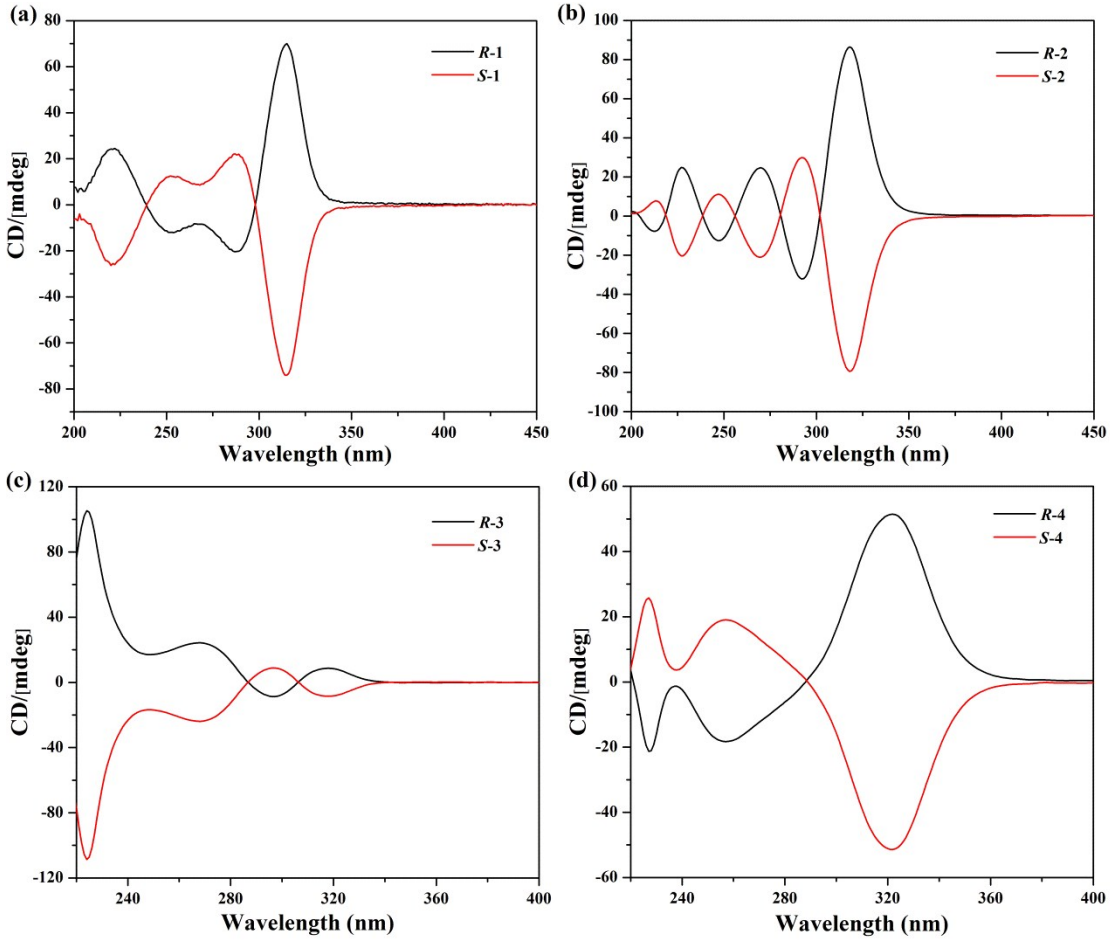

Figure S1. CD spectra of the pairs of enantiomers (0.02 mM) of tetrahedral cages (a) ***R*-1**/***S*-1**, (b) ***R*-2**/***S*-2**, (c) ***R*-3**/***S*-3**, (d) ***R*-4**/***S*-4**.

4. Crystal morphologies

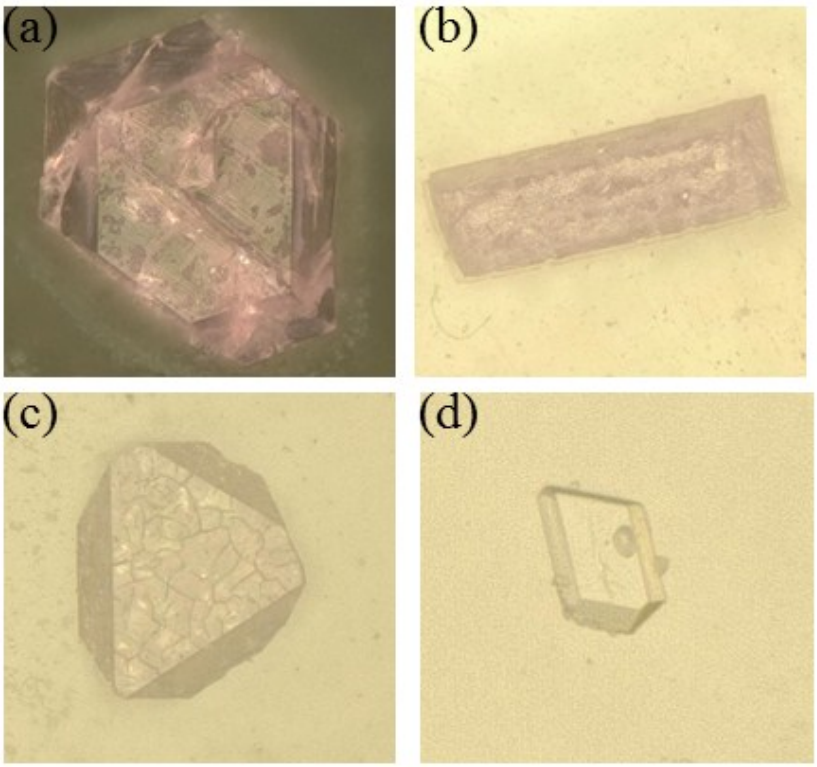

Figure S2. Crystal morphologies of cages (a) *ΛΛΛΛ*-$[Ni_4(R\text{-}L^1)_6][ClO_4]_8$, (b) *ΔΔΔΔ*-$[Ni_4(S\text{-}L^2)_6][BF_4]_8$, (c) *ΔΔΔΔ*-$[Ni_4(S\text{-}L^3)_6]Cl_8$, (d) *ΛΛΛΛ*-$[Ni_4(R\text{-}L^4)_6][SO_3CF_3]_8$.

5. Crystal structural figures

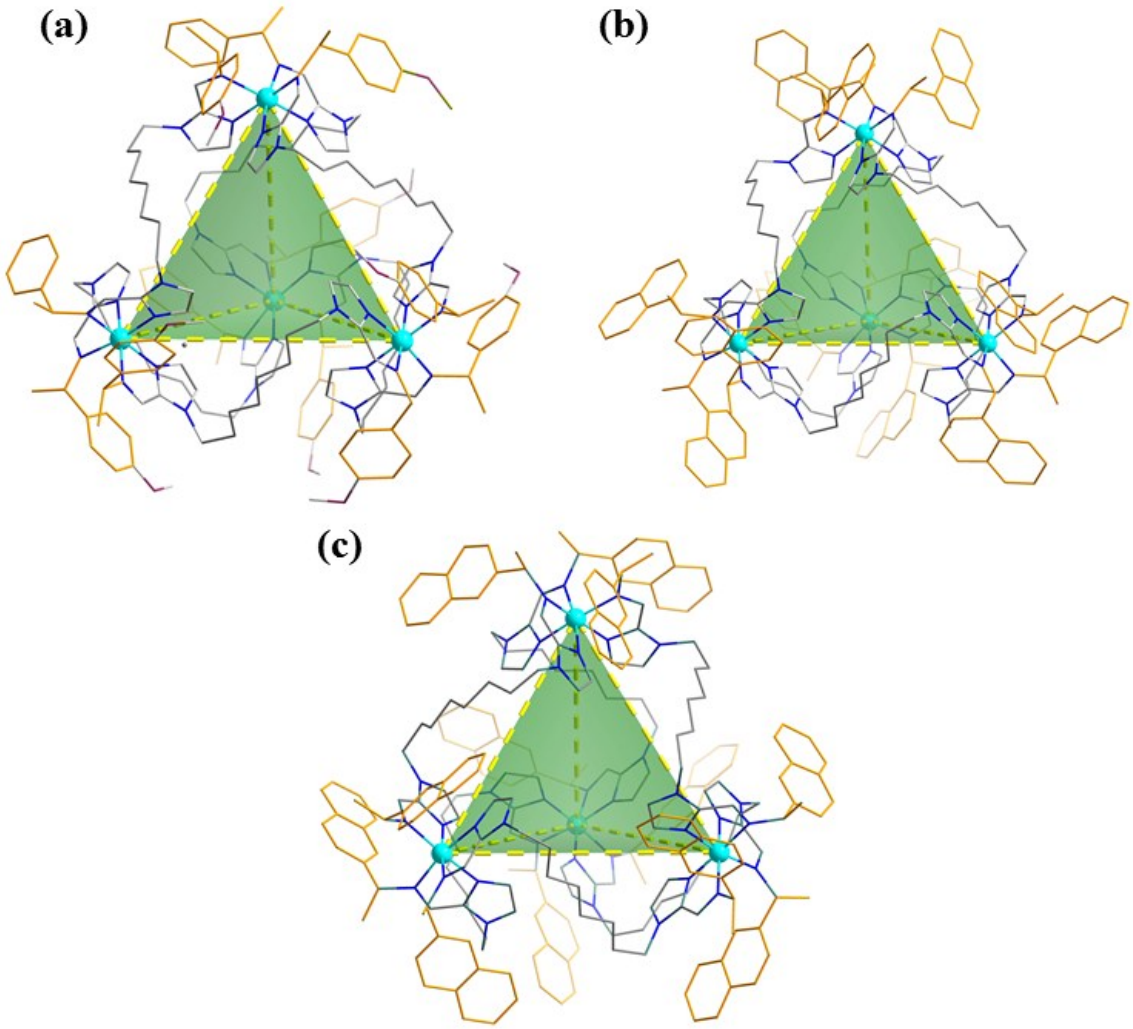

Figure S3. X-ray crystal structures of tetrahedral cages (a) *ΔΔΔΔ*-$[Ni_4(S\text{-}L^2)_6][BF_4]_8$, (b) *ΔΔΔΔ*-$[Ni_4(S\text{-}L^3)_6]Cl_8$, (c) *ΛΛΛΛ*-$[Ni_4(R\text{-}L^4)_6][SO_3CF_3]_8$. All H atoms and anions have been removed for clarity.

6. Stability in aqueous media

Visible absorbance spectra for stability studies were recorded using a Shimadzu UV-2101 PC scanning spectrometer. Measurements were collected in a 1 cm path-length cuvette and the standard parameters used were bandwidth 1 nm, response time 1 sec, wavelength scan range 200-600 nm. Visible absorbance spectra for each sample were repeated at least three times. The intensity of the band (200-300 nm) of a 0.02 mM solution of each cage was measured over time in 0.2 M hydrochloric acid at 20 °C (every 2 h for 24 h), since peaks for decomposition products are unlikely to appear in this region. The half-lives ($t_{½}$) were calculated using the following equations:

$$\ln[A] = -kt + \ln[A]_0 \qquad t_{½} = \frac{\ln(2)}{k}$$

Table S1. Solution half-life ($t_{1/2}$) for the chloride cages (0.02 mM) in 0.2 M hydrochloric acid at 20 °C.

compound	$t_{½}$/h
***R*-1**	0.2
***S*-1**	0.2
***R*-2**	0.8
***S*-2**	1.2
***R*-3**	18.9
***S*-3**	19.0
***R*-4**	15.5
***S*-4**	15.1

7. UV-vis study of cages interacting with HTG22 DNA

UV-vis absorption spectra were collected on a Shimadzu UV-2101 PC scanning spectrophotometer. The spectra of the cages were recorded after successive additions of DNA solutions (HTG22 in Na^+ buffer and K^+ buffer: from 0 to 2.0 μM). During the titration, the same volume buffered DNA solution was added to each cuvette (1.0 cm path length) to eliminate the absorbance of DNA itself, and the solutions were mixed by repeated inversion. The absorption spectra were recorded after mixing for 5 min, and the UV-vis titrations for each sample were repeated at least three times. The binding constants (K_b) of the cages were determined by fitting the data to a plot of [DNA]/(ε_f–ε_a) versus [DNA] using the following equation[2]:

$$[D]/\Delta\varepsilon_{ap} = [D]/\Delta\varepsilon + 1/(K_b \times \Delta\varepsilon),\ \Delta\varepsilon_{ap} = |\varepsilon_a - \varepsilon_f|,\ \Delta\varepsilon = |\varepsilon_b - \varepsilon_f|$$

Where ε_f and ε_b correspond to the molar extinction coefficients of free and DNA-bound complex respectively, and ε_a is the apparent molar extinction coefficient (absorbance at λ_{max} of complex/concentration of complex).

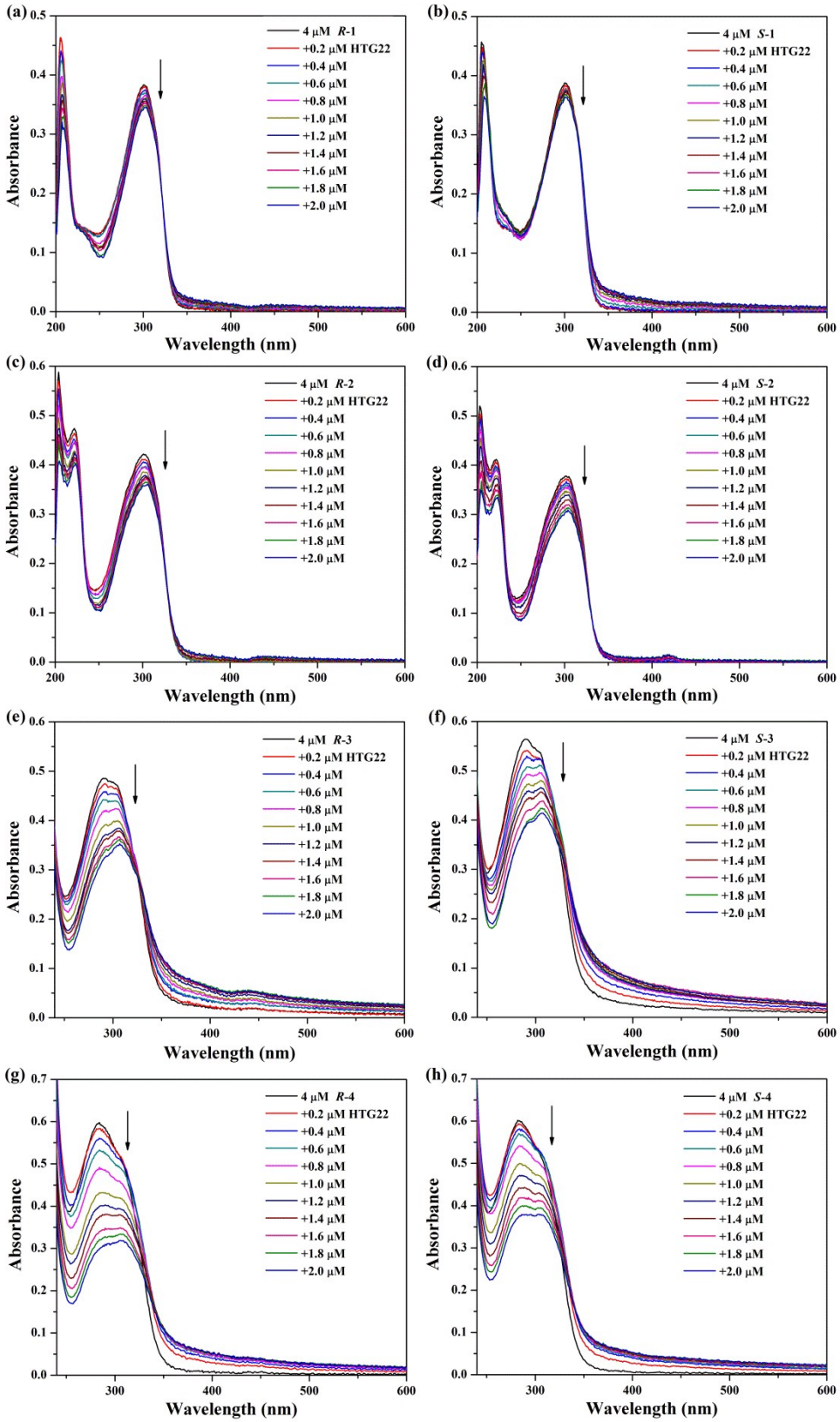

Figure S4. UV-vis spectra of cages (a) ***R*-1**, (b) ***S*-1**, (c) ***R*-2**, (d) ***S*-2**, (e) ***R*-3**, (f) ***S*-3**, (g) ***R*-4**, (h) ***S*-4** with increasing concentration of HTG22 in Na^+ buffer (100 mM NaCl, 10 mM Tris-HCl, pH = 7.4).

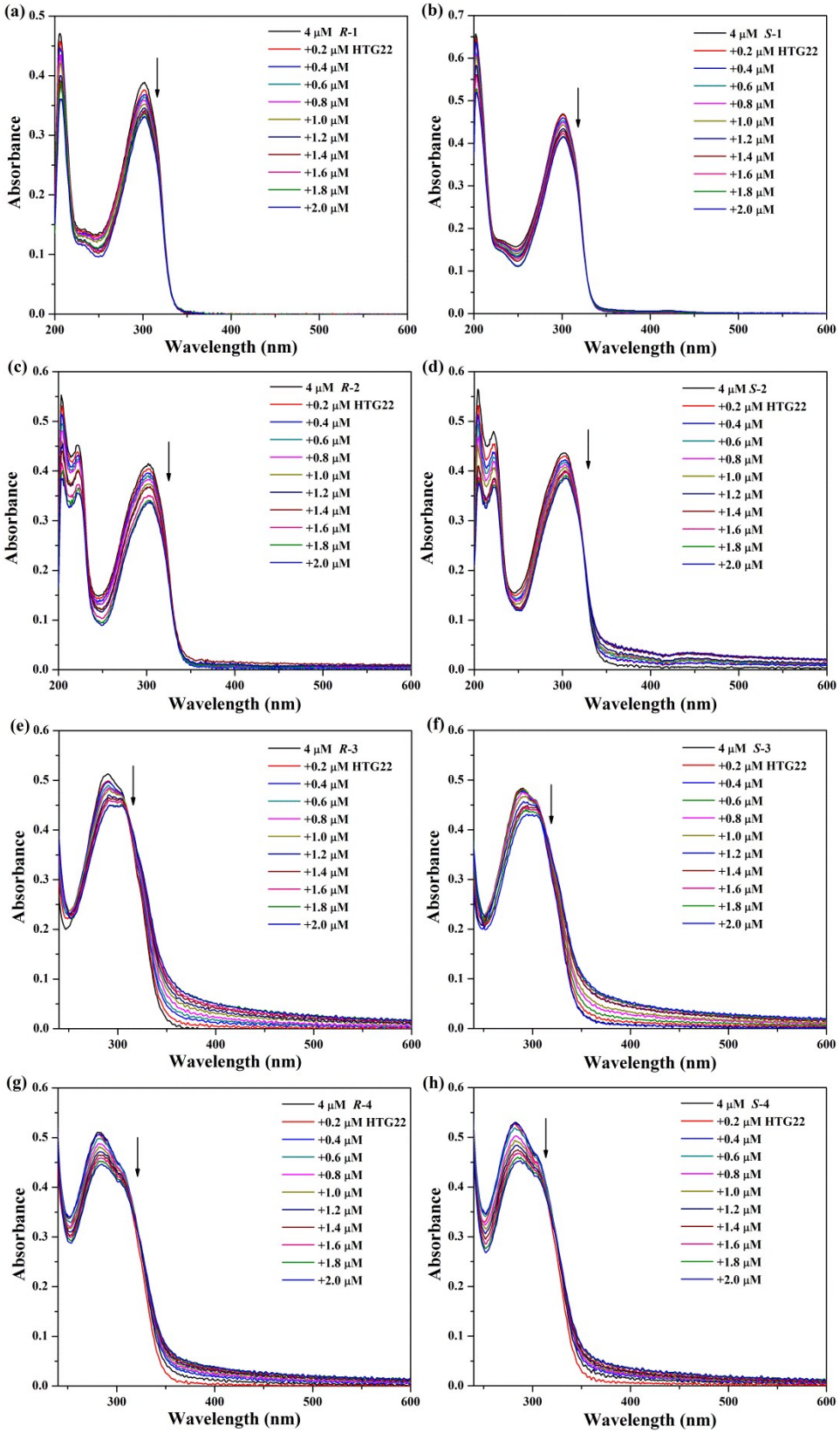

Figure S5. UV-vis spectra of cages (a) ***R*-1**, (b) ***S*-1**, (c) ***R*-2**, (d) ***S*-2**, (e) ***R*-3**, (f) ***S*-3**, (g) ***R*-4**, (h) ***S*-4** with increasing concentration of HTG22 in K^+ buffer (100 mM KCl, 10 mM Tris-HCl, pH = 7.4).

8. CD titrations

A circular dichroism titration series was conducted to investigate the effect of the cages on the structure of the G-quadruplex. CD studies were carried out using a MOS-450/AF-CD spectro polarimeter at room temperature. HTG22 was prepared in Na^+ buffer and heated at 95 °C for 5 min and left to cool at room temperature overnight to obtain the intramolecular quadruplex structure. The various concentration of each enantiomer was scanned as a control and subtracted from the spectra of cages/DNA mixture to eliminate its influence on DNA CD signal. For each sample 5 min was allowed for equilibration. Three scans were accumulated and automatically averaged. This experiment was also repeated in K^+ buffer with similar results.

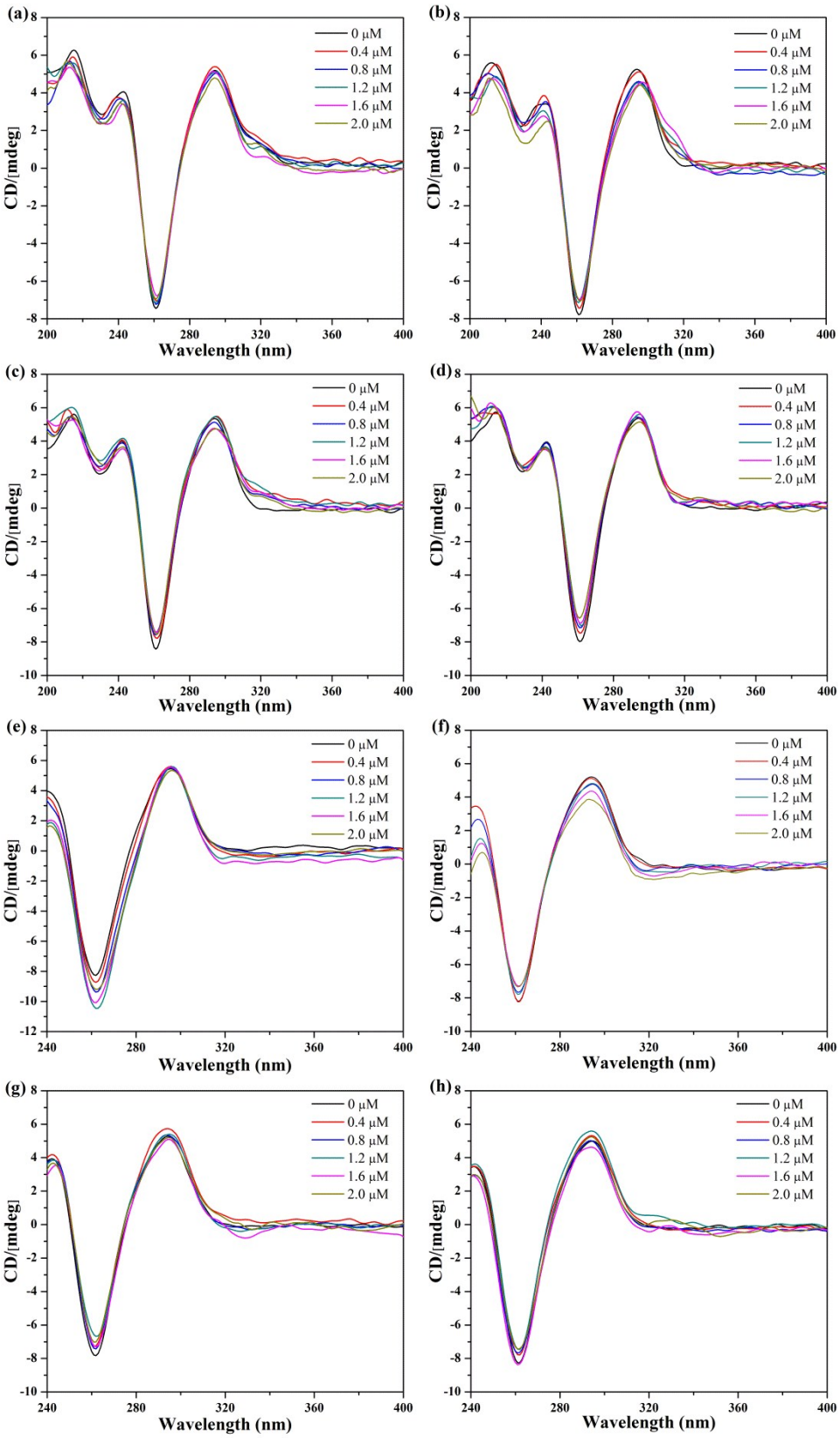

Figure S6. CD spectra of HTG22 (2 μM) induced by cages (a) ***R*-1**, (b) ***S*-1**, (c) ***R*-2**, (d) ***S*-2**, (e) ***R*-3**, (f) ***S*-3**, (g) ***R*-4**, (h) ***S*-4** in Na^+ buffer (100 mM NaCl, 10 mM Tris-HCl, pH = 7.4).

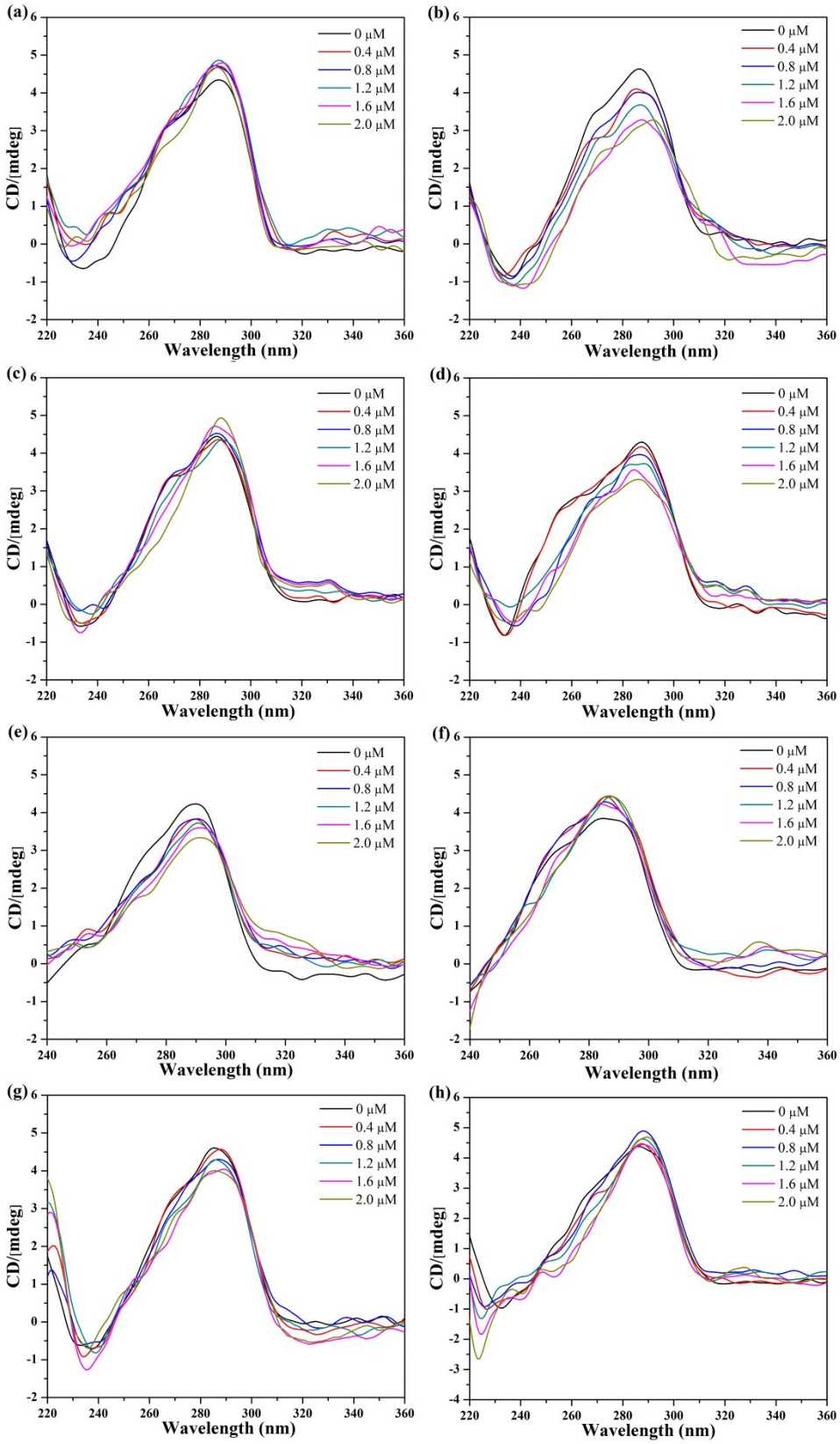

Figure S7. CD spectra of HTG22 (2 μM) induced by cages (a) ***R*-1**, (b) ***S*-1**, (c) ***R*-2**, (d) ***S*-2**, (e) ***R*-3**, (f) ***S*-3**, (g) ***R*-4**, (h) ***S*-4** in K^+ buffer (100 mM KCl, 10 mM Tris-HCl, pH = 7.4).

9. Thermal stabilities of cages

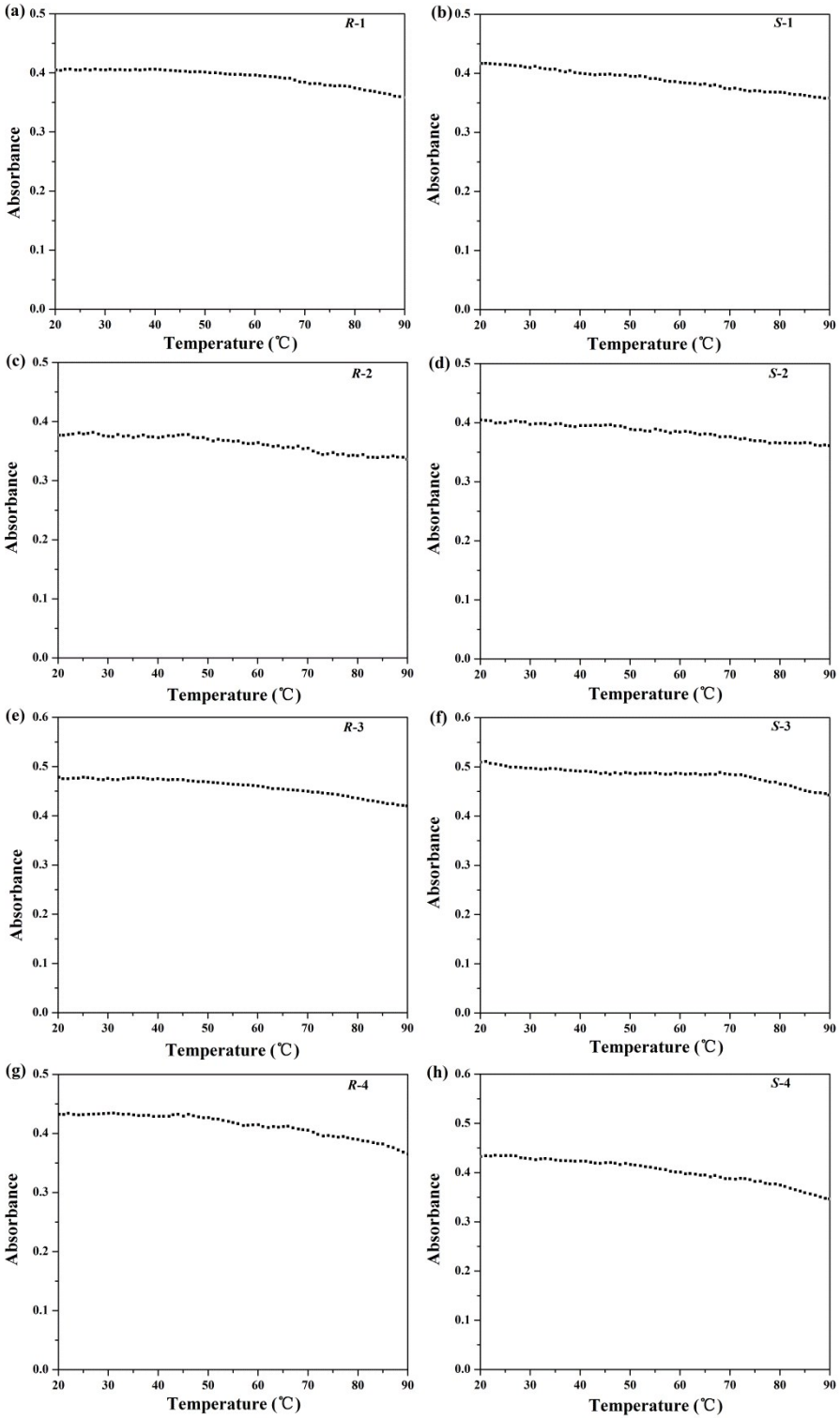

Figure S8. Thermal stabilities of cages (4 μM): (a) ***R*-1**, (b) ***S*-1**, (c) ***R*-2**, (d) ***S*-2**, (e) ***R*-3**, (f) ***S*-3**, (g) ***R*-4**, (h) ***S*-4**. Absorbance is measured at 300 nm. Experiments were carried out in water at 1 °C·min^{-1} temperature gradient.

10. Melting temperature measurements

The fluorescent-labeled oligonucleotide, F22T, was used as the FRET probes. Fluorescence melting curves were measured on a Bio-Rad iQ5 real-time PCR detection system by using a total reaction volume of 25 μL with 0.2 μM of labeled oligonucleotide and different concentrations of cages. Fluorescence readings with excitation were taken at intervals of 1 °C in the temperature range of 20-90 °C, with a constant temperature being maintained for 30 s before each reading to ensure the sample had reached equilibrium. The melting of the G-quadruplex was monitored alone or in the presence of various concentrations of cages. Competitive FRET-melting experiments were carried out with F22T in Na^+ buffer and K^+ buffer. All of the conditions of the reaction system were similar to those used in the FRET melting except that different concentrations of duplex DNA ds26 were added. Final analysis of the data was carried out using Origin 7.5 software (Origin Lab Corp.).

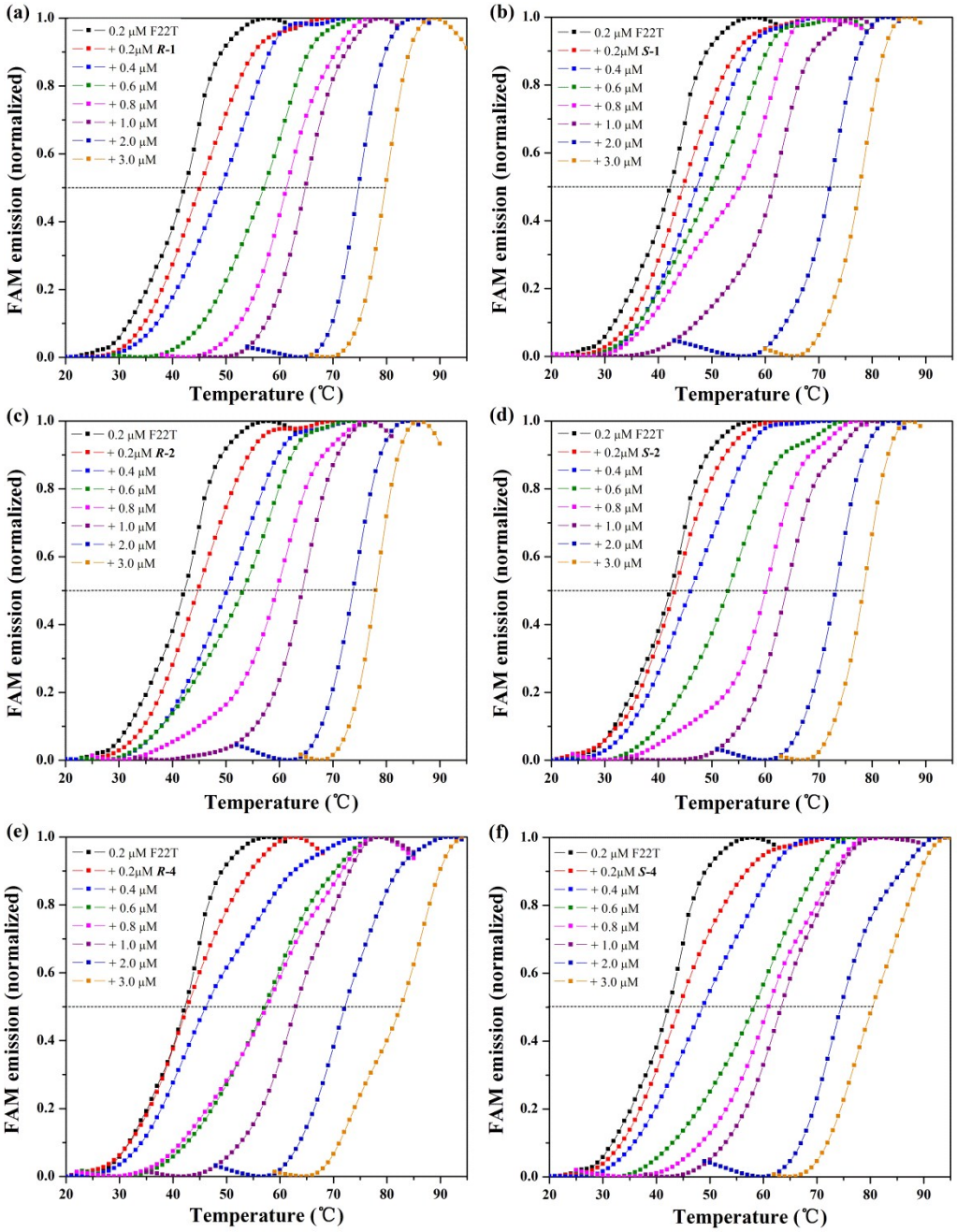

Figure S9. FRET melting profiles of 0.2 μM F22T with different cages (a) ***R*-1**, (b) ***S*-1**, (c) ***R*-2**, (d) ***S*-2**, (e) ***R*-4**, (f) ***S*-4** in Na^+ buffer (100 mM NaCl, 10 mM Tris-HCl, pH = 7.4).

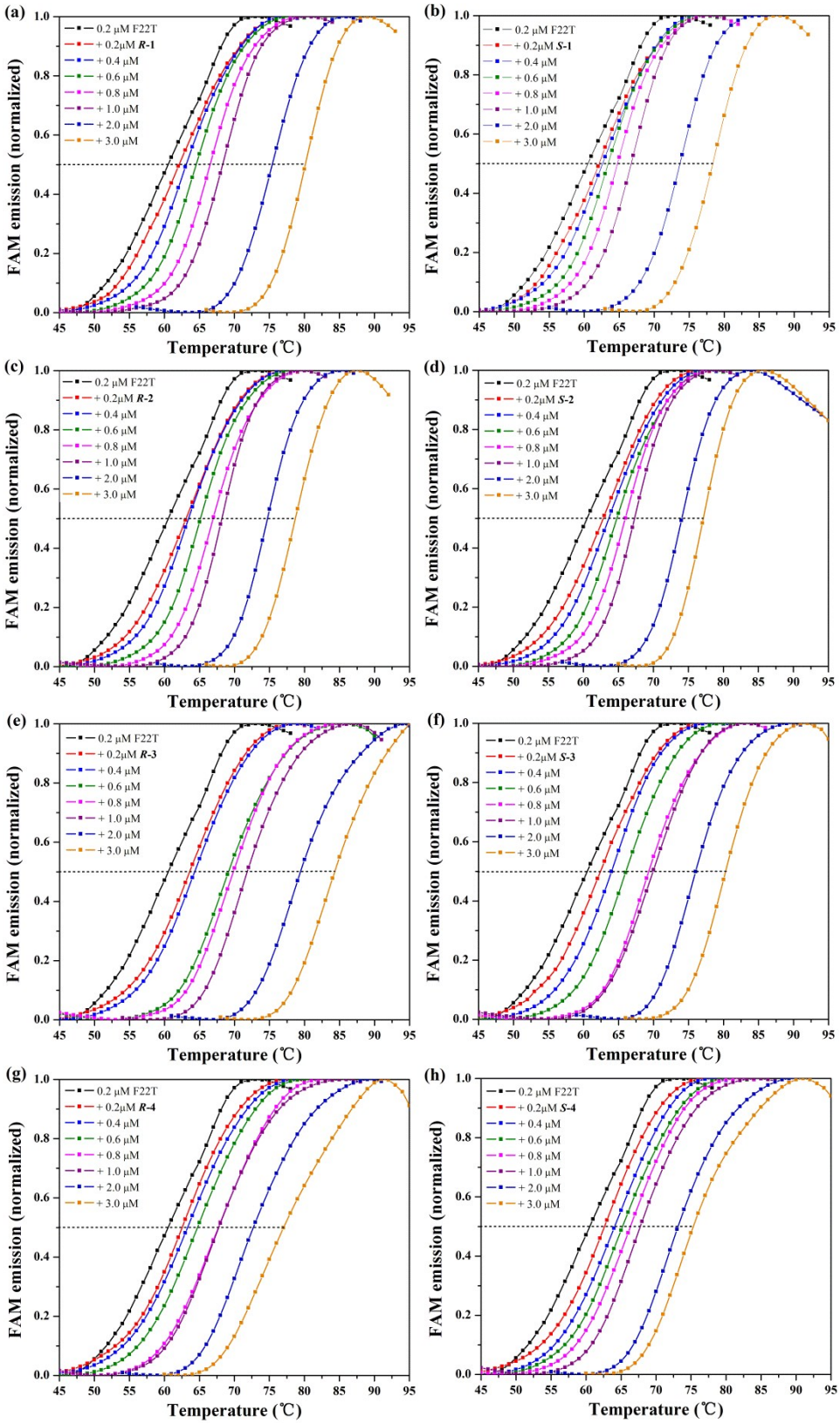

Figure S10. FRET melting profiles of 0.2 μM F22T with different cages (a) ***R*-1**, (b) ***S*-1**, (c) ***R*-2**, (d) ***S*-2**, (e) ***R*-3**, (f) ***S*-3**, (g) ***R*-4**, (h) ***S*-4** in K^+ buffer (100 mM KCl, 10 mM Tris-HCl, pH = 7.4).

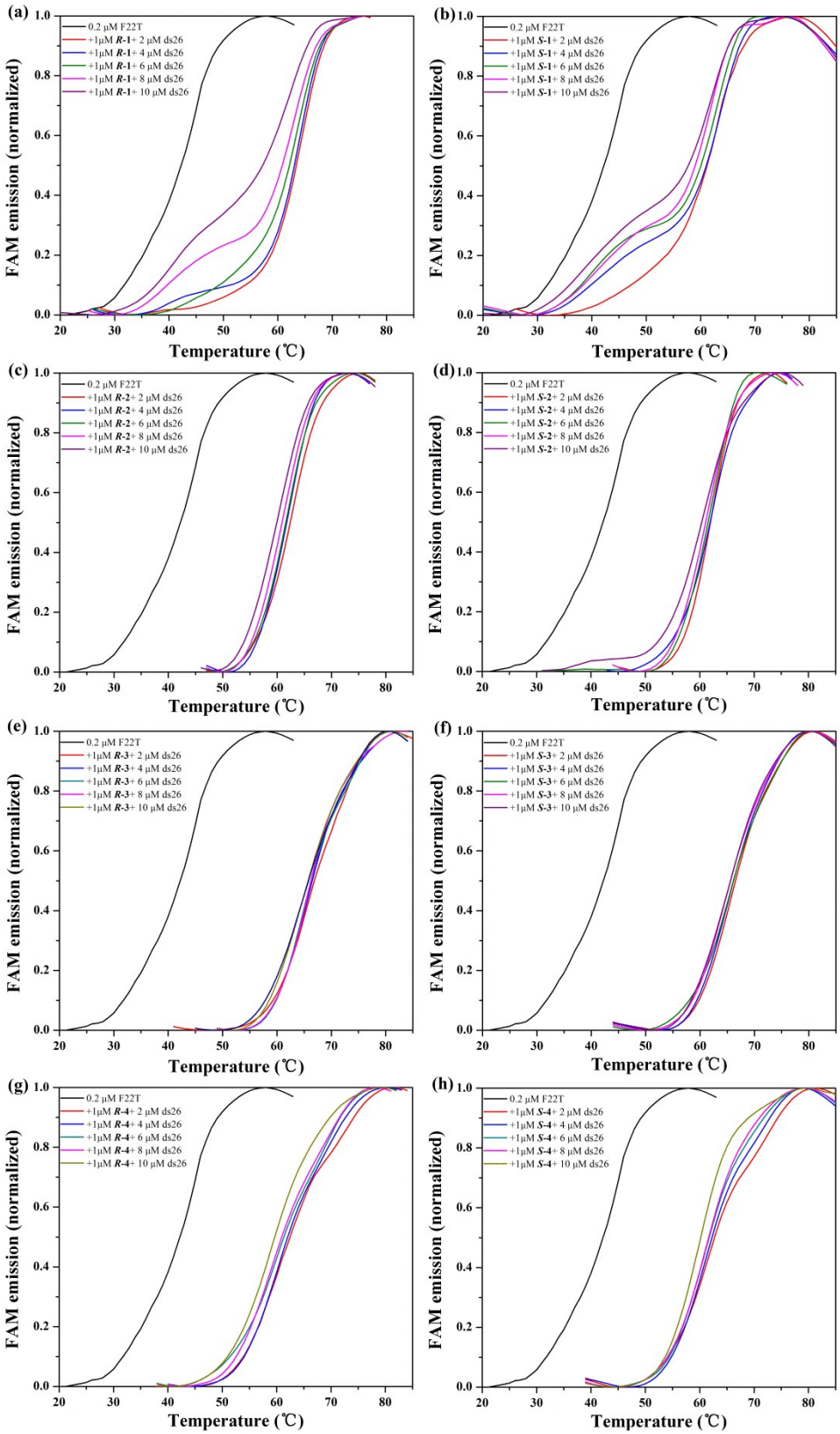

Figure S11. FRET results (T_m, °C) for cages (1 μM): (a) ***R*-1**, (b) ***S*-1**, (c) ***R*-2**, (d) ***S*-2**, (e) ***R*-3**, (f) ***S*-3**, (g) ***R*-4**, (h) ***S*-4** in absence or presence of different concentrations of competitive ds26 in Na^+ buffer (100 mM NaCl, 10 mM Tris-HCl, pH = 7.4).

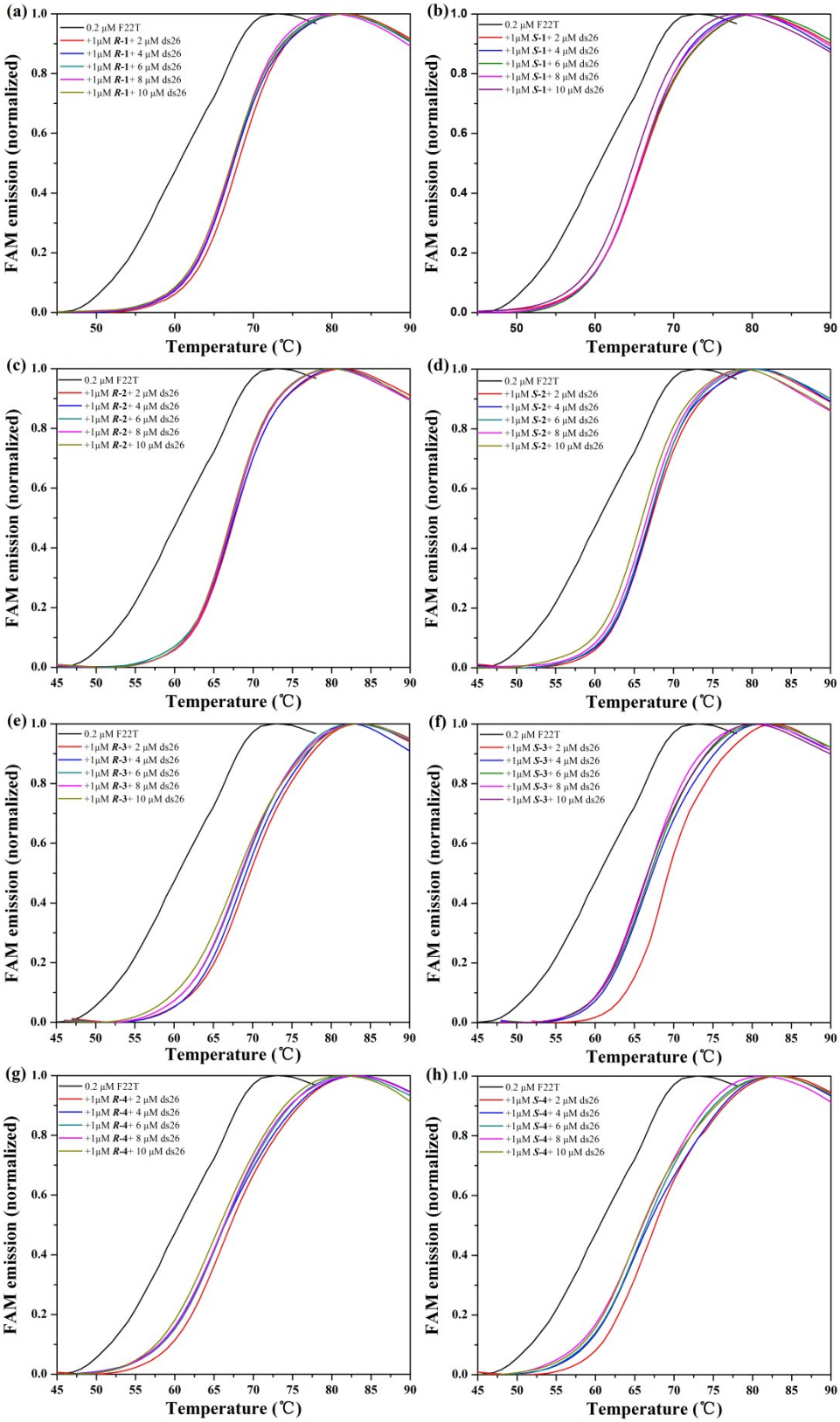

Figure S12. FRET results (T_m, °C) for cages (1 μM): (a) ***R*-1**, (b) ***S*-1**, (c) ***R*-2**, (d) ***S*-2**, (e) ***R*-3**, (f) ***S*-3**, (g) ***R*-4**, (h) ***S*-4** in absence or presence of different concentrations of competitive ds26 in K^+ buffer (100 mM KCl, 10 mM Tris-HCl, pH = 7.4).

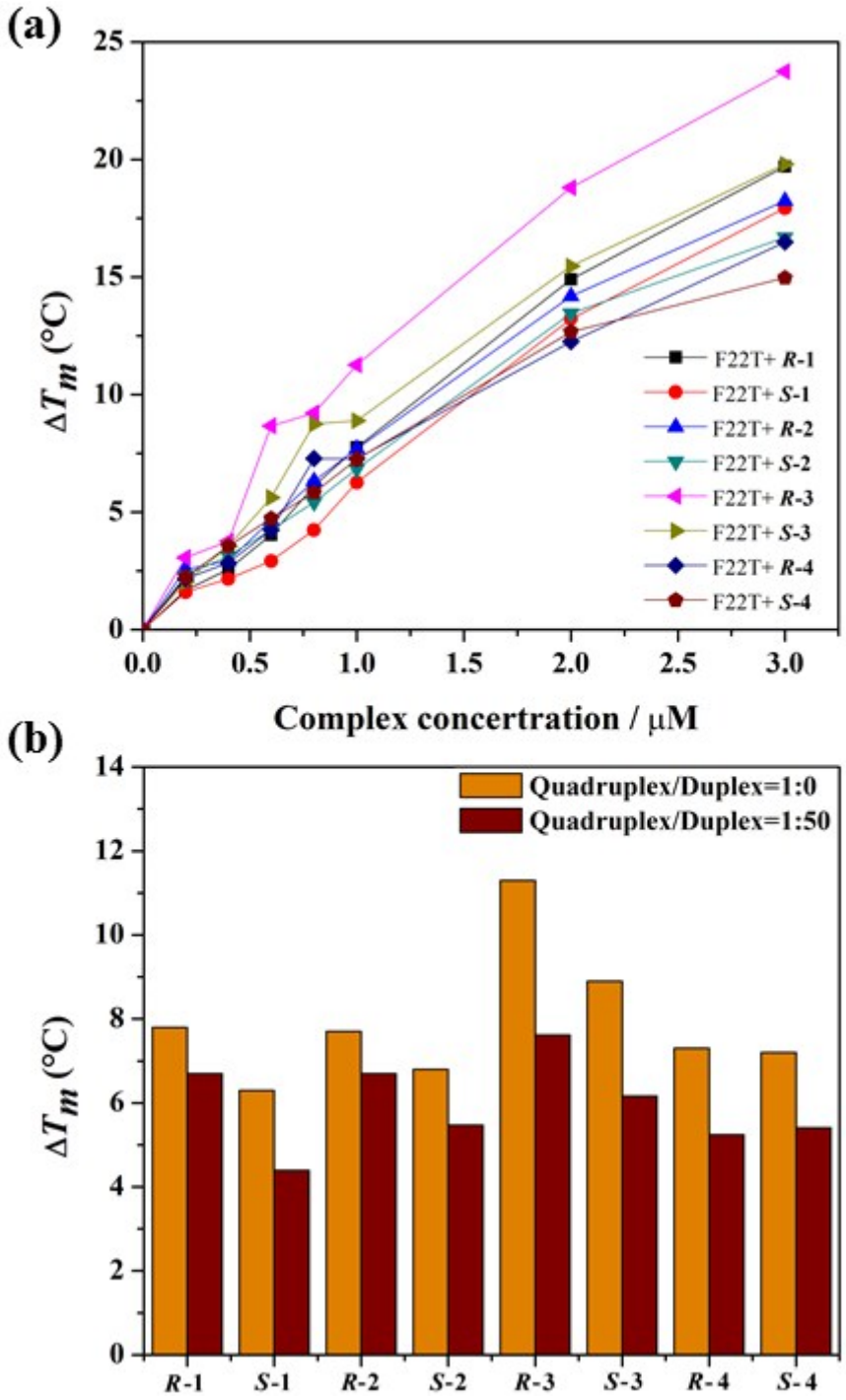

Figure S13. (a) Plot of ΔT_m versus the concentration of cages. (b) Competition FRET experiment in the presence of 1 μM of cages with various concentration of ds26. All measurements were performed in K^+ buffer.

11. Continuous variation analysis

Binding stoichiometries were obtained using the method of continuous variation[3], equimolecular solutions of cages and G-quadruplex DNA are mixed in various proportions. The mole fraction of each cage was varied from 0.1 to 1.0, in 0.1 increments, while the total concentration was kept at 5 μM. The difference (ΔA) between each experimental value and that calculated as the sum of the contributions of the two separate components is plotted against the molar fractions. The resulting curves display a break point at the molar fraction corresponding to the stoichiometry of the complex. The absorption of each sample was recorded at room temperature and baseline values were routinely subtracted from the spectra.

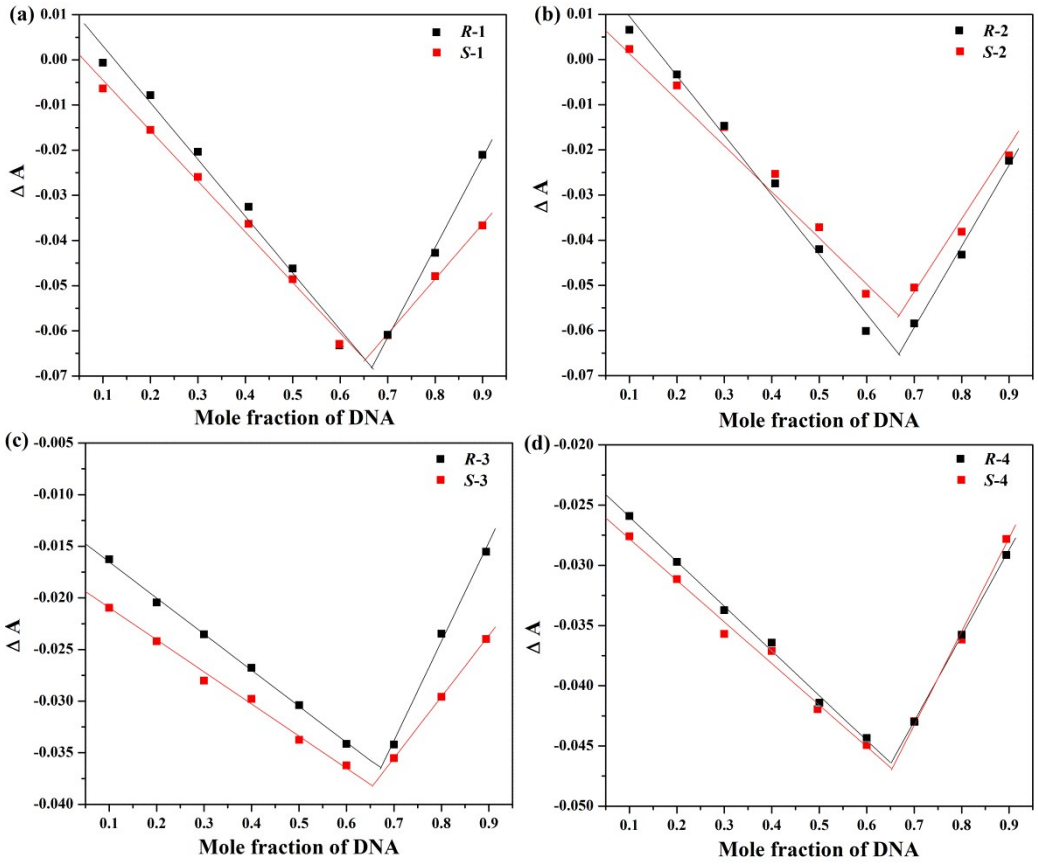

Figure S14. Job plots for the binding of cages (a) ***R*-1/*S*-1**, (b) ***R*-2/*S*-2**, (c) ***R*-3/*S*-3**, (d) ***R*-4/*S*-4** to G-quadruplex DNA in Na^+ buffer (100 mM NaCl, 10 mM Tris-HCl, pH = 7.4).

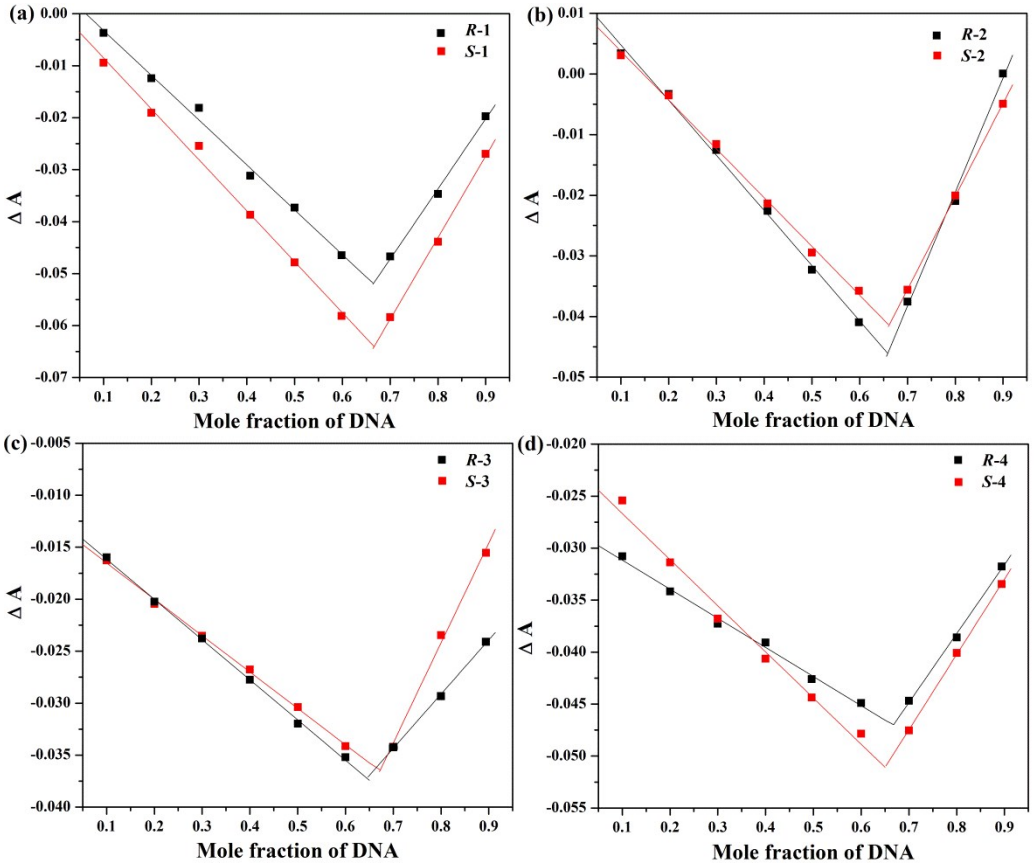

Figure S15. Job plots for the binding of cages (a) ***R*-1/*S*-1**, (b) ***R*-2/*S*-2**, (c) ***R*-3/*S*-3**, (d) ***R*-4/*S*-4** to G-quadruplex DNA in K^+ buffer (100 mM KCl, 10 mM Tris-HCl, pH = 7.4).

12. Cytotoxicity assay

Three human cancer cell lines (HCT116, MCF-7 and HepG2) were cultured in the DMEM medium supplemented with 10% FBS, 100 μg/mL penicillin and 100 μg/mL streptomycin. All these cells were plated into 96-well plates (100 μL per well) at the density of 5-6 × 10^4 cells/mL, and incubated in a humidified atmosphere of 5% CO_2 and 95% air at 37 °C for 24 h, which allowed for the cell attachment. The stock solutions (10 mM) were prepared by dissolving the cages in DMSO. The final concentration of DMSO in each well was 5‰ and the culture medium with 5‰ DMSO was used as a control. Cages were dissolved to the indicated concentration and mixed with the culture medium, which were further incubated for 48 h and 96 h, respectively. In order to evaluate the morphological changes of these cancer cell lines, the cells were observed under the inverted light microscope and photographed by a Panasonic Lumix DMC-FH2. At the end of incubation period, 20 μL 3-(4,5-dimethylthiazol-2-yl)-2,5-diphenyltetrazolium bromide (MTT) solution (5 mg/ml) was added to each well and then the plates were incubated for another 4 h. Subsequently, the supernatant was removed after centrifugation and 150 μL DMSO was added to each well for dissolving the formazan crystal. The absorbance was measured at the wavelength of 490 nm using a microplate reader (BioTek Instruments, Inc. Vermont, USA). The IC_{50} values were determined and defined as the concentration of cages that is required for inhibiting cells by 50%. All experiments were performed at least three times, and the results were presented as mean ± SD.

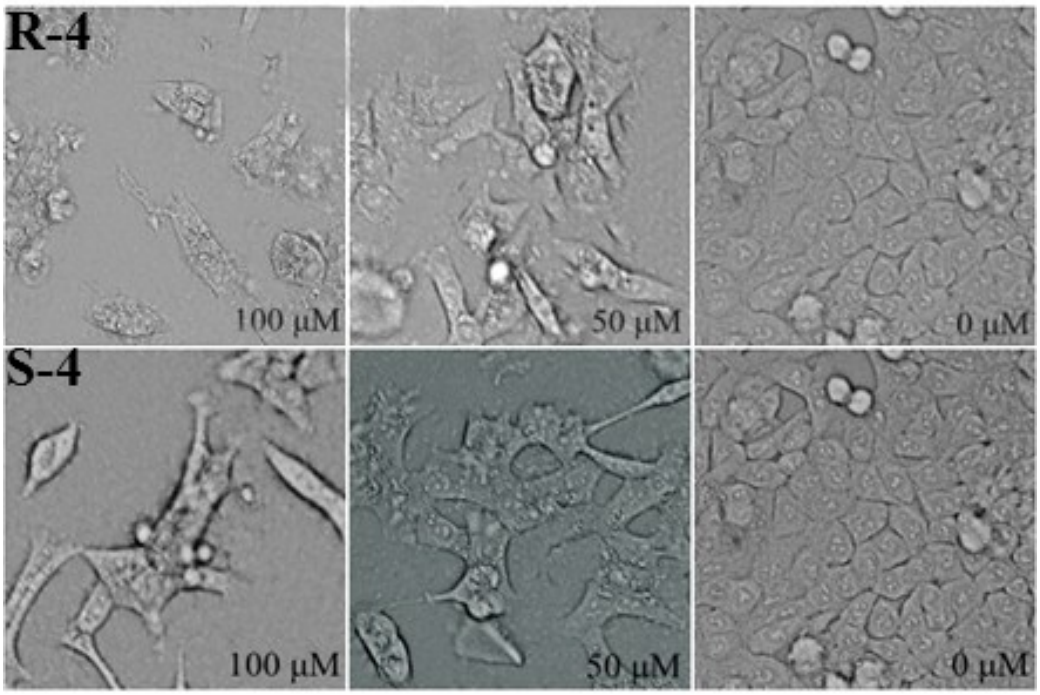

Figure S16. Morphological changes of cancer cell lines HCT116 treated by cages ***R*-4** and ***S*-4** for 48 h at the indicated concentration.

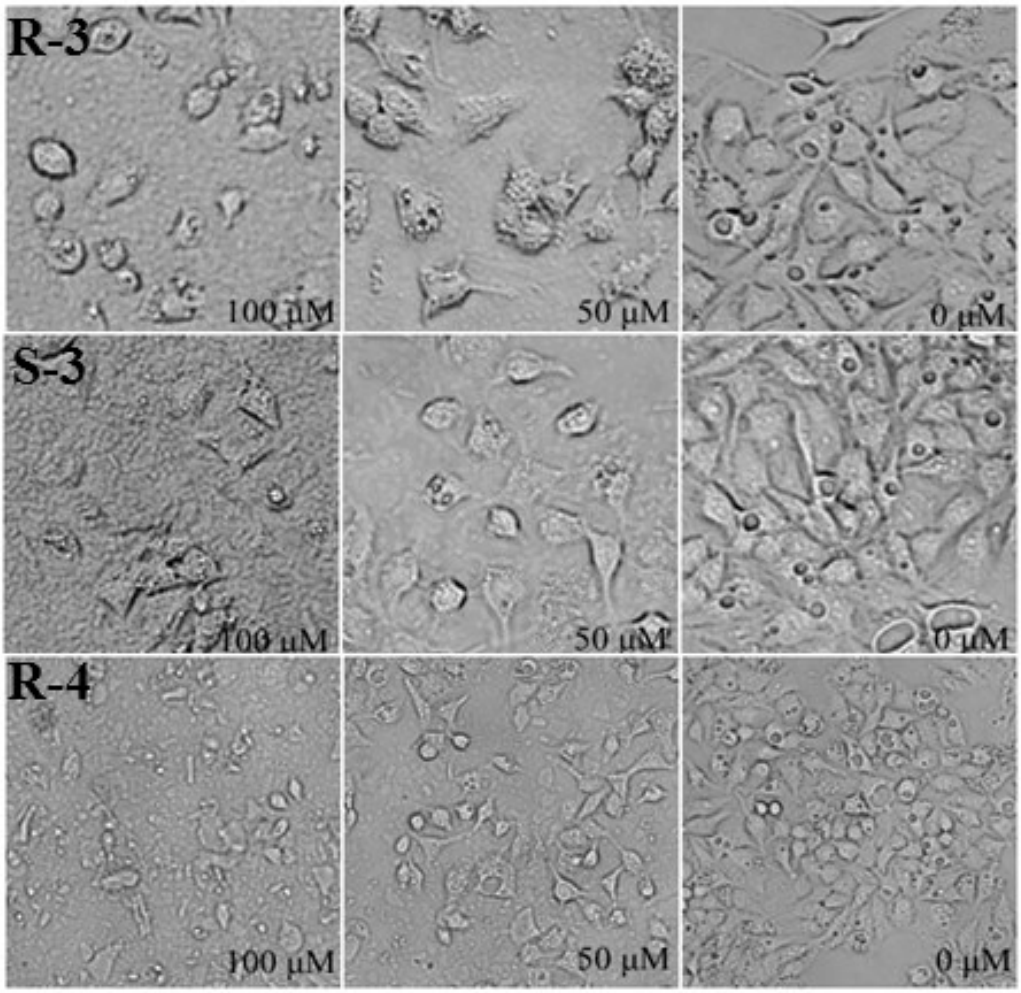

Figure S17. Morphological changes of cancer cell lines HepG2 treated by cages ***R*-3**, ***S*-3** and ***R*-4** for 48 h at the indicated concentration.

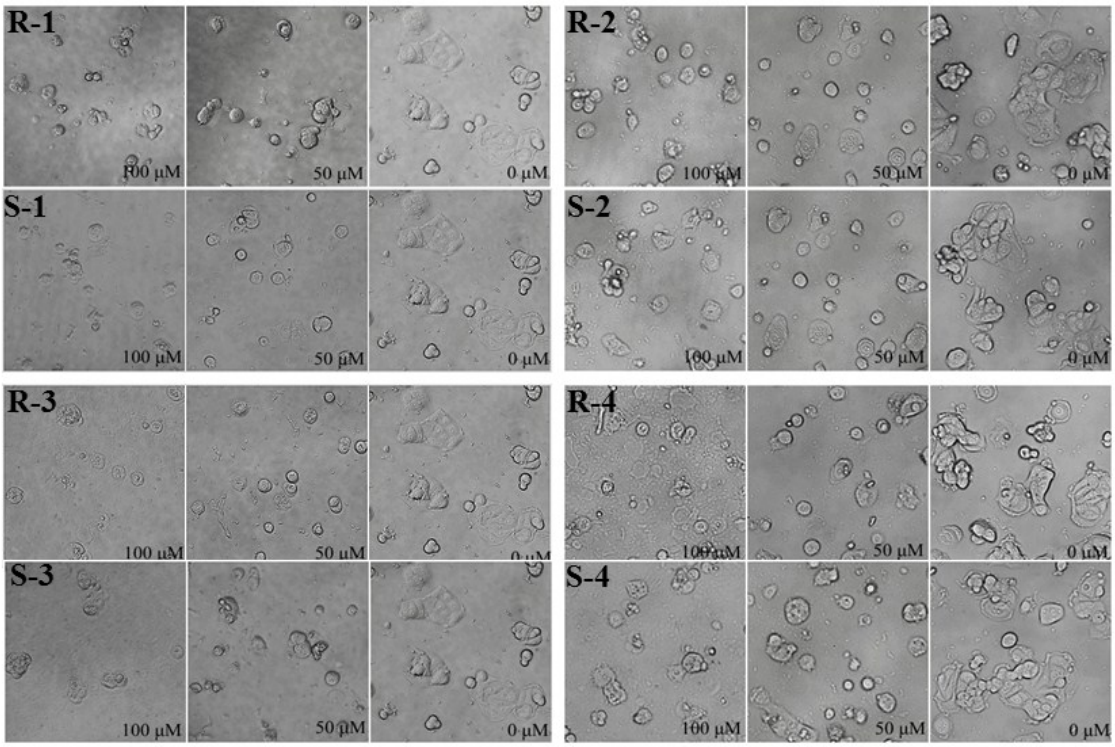

Figure S18. Morphological changes of cancer cell lines MCF-7 treated by cages for 48 h at the indicated concentration.

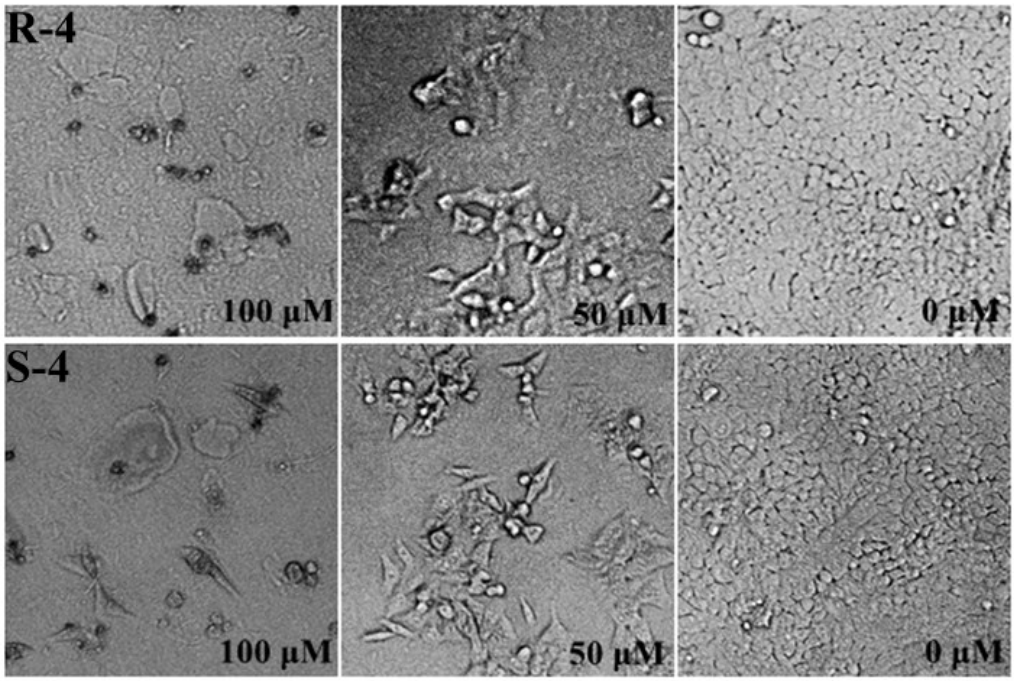

Figure S19. Morphological changes of cancer cell lines HCT116 treated by cages ***R*-4** and ***S*-4** for 96 h at the indicated concentration.

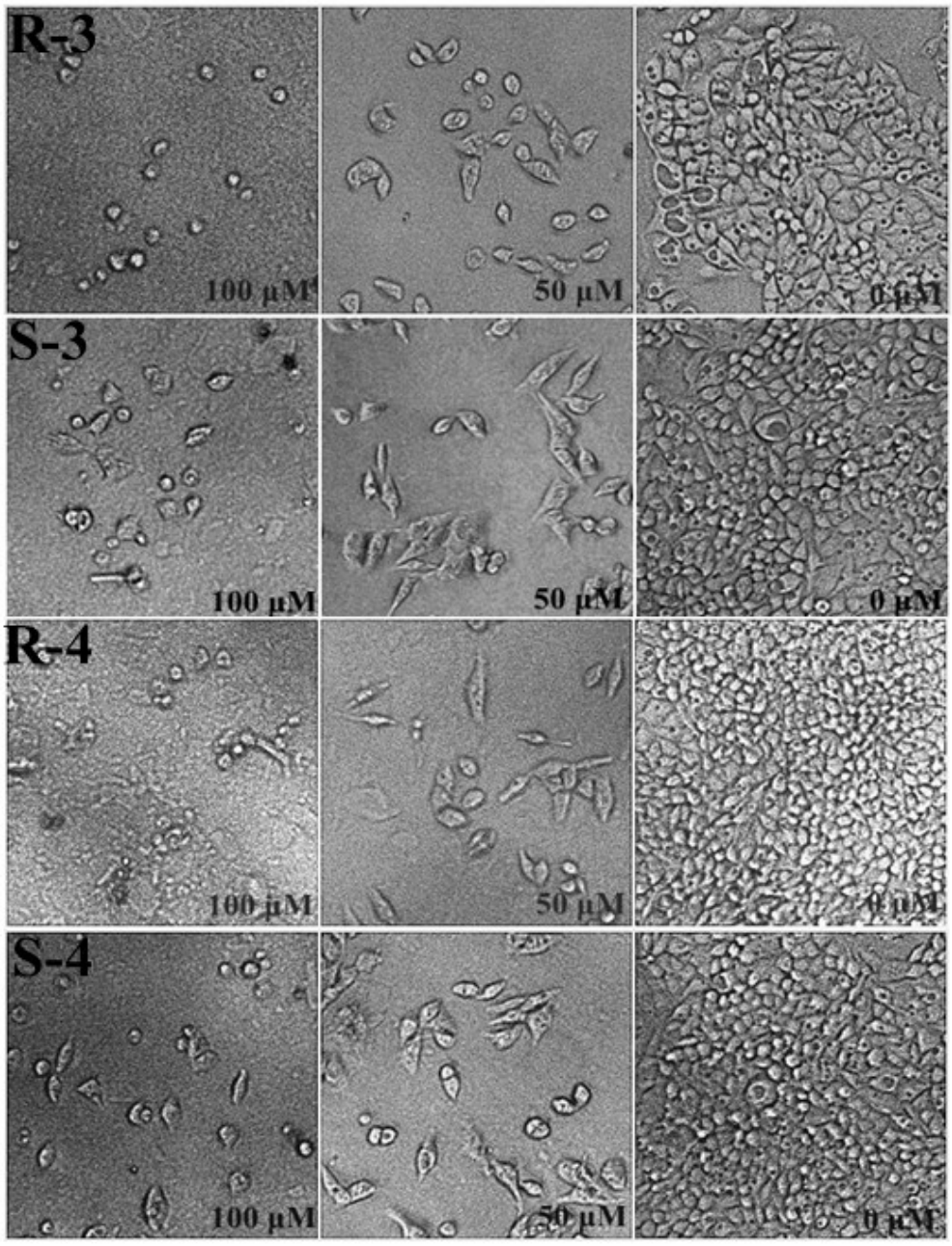

Figure S20. Morphological changes of cancer cell lines HepG2 treated by cages ***R*-3**, ***S*-3**, ***R*-4** and ***S*-4** for 96 h at the indicated concentration.

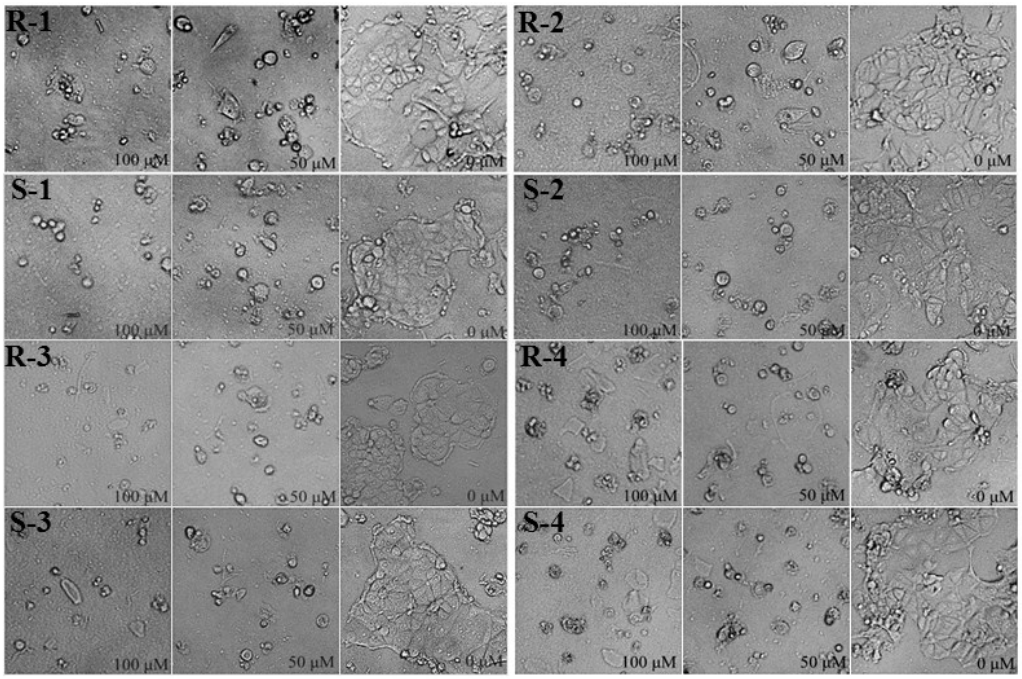

Figure S21. Morphological changes of cancer cell lines MCF-7 treated by cages for 96 h at the indicated concentration.

Table S2. IC_{50} values [μM] obtained for the cages against HCT116, HepG2, and MCF-7 cell lines tested at 96 h. The values presented as mean±SD of three independent experiments.

compound	$IC_{50}/\mu M$		
	HCT-116	HepG2	MCF-7
***R*-1**	—	—	36.51±1.10
***S*-1**	—	—	25.91±0.46
***R*-2**	—	—	36.85±0.82
***S*-2**	—	—	39.37±0.31
***R*-3**	—	34.14±0.27	28.53±0.37
***S*-3**	—	42.19±0.49	27.36±0.07
***R*-4**	35.06±0.52	35.36±1.03	32.37±0.99
***S*-4**	34.76±0.66	41.25±0.24	39.87±0.51

13. Determination of apoptotic cells by flow cytometric analysis

The ability of ***S*-1** to induce apoptosis in tumour cell lines was assessed by propidium iodide (PI) staining and flow cytometric analysis. The MCF-7 cells were grown in six-well plates at a density of 4×10^5 cells/well and incubated for 24 h at 37 °C in a CO_2 incubator. Then, cells were exposed to 35 μM ***S*-1** for 48 h. After 48 h treatment, the medium was removed and the cells washed with PBS and trypsinized. Then the cells were fixed in 70% ethanol by incubation at 4 °C for 12 h. After centrifugation, ethanols were decanted and the cell pellets were resuspended in 200 μL PBS solution containing PI (50 μg/mL) and RNase A (50 μg/mL). After 30 min incubation at room temperature, the samples were acquired in a flow cytometer, FACS Calibur (BD Biosciences, CA, USA). The distribution of cells in different phases of cell cycle was estimated using the ModFit32 software. The percentage of apoptotic cells was determined by the sub-G1 peak in the DNA histogram.

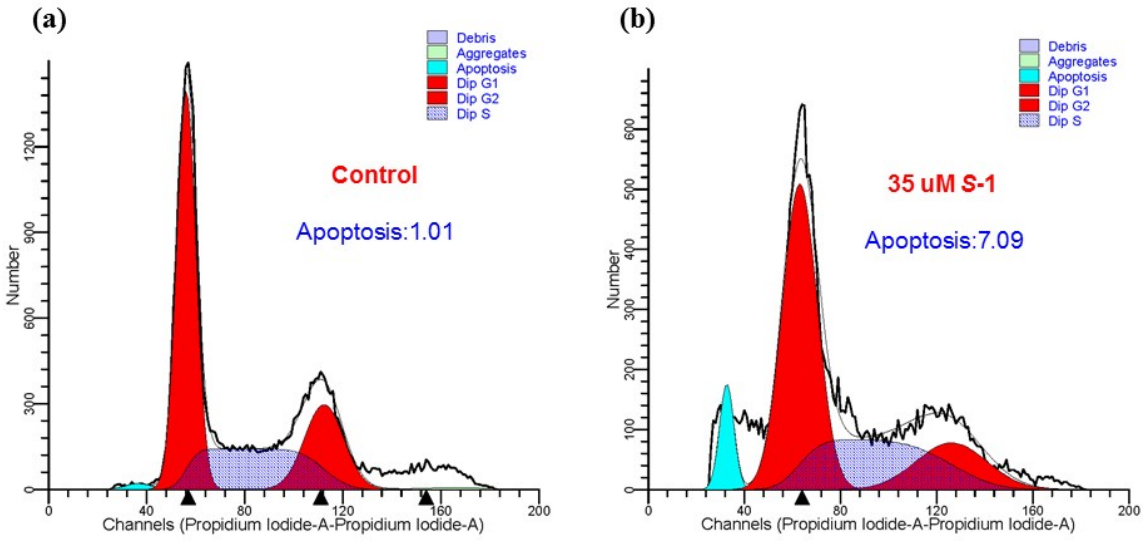

Figure S22. Cell cycle progression analysis of ***S*-1** treated MCF-7 cells for 48 h.

14. X-ray crystallography data

The crystal structures were determined on a Siemens (Bruker) SMART CCD diffractometer using monochromated Mo $K\alpha$ radiation (λ = 0.71073 Å) at 173(2) K. Cell parameters were retrieved using SMART software and refined using SAINT[4] on all observed reflections. The highly redundant data sets were reduced using SAINT and corrected for Lorentz and polarization effects. Data was collected using a narrow-frame method with scan widths of 0.30° in ω and an exposure time of 10 s/frame. Absorption corrections were applied using SADABS[5] supplied by Bruker. Structures were solved by direct methods using the program SHELXL-97[6]. All of the non-hydrogen atoms except the disordered solvent molecules and anions were refined with anisotropic thermal displacement coefficients. Hydrogen atoms of organic ligands were located geometrically and refined in a riding model, whereas those of solvent molecules were not treated during the structural refinements. Disorder was modelled using standard crystallographic methods including constraints, restraints and rigid bodies where necessary. The crystals of the cages *ΛΛΛΛ*-$[Ni_4(R\text{-}L^1)_6][ClO_4]_8$, *ΔΔΔΔ*-$[Ni_4(S\text{-}L^1)_6][ClO_4]_8$, *ΔΔΔΔ*-$[Ni_4(S\text{-}L^2)_6][BF_4]_8$, *ΔΔΔΔ*-$[Ni_4(S\text{-}L^3)_6]Cl_8$ and *ΛΛΛΛ*-$[Ni_4(R\text{-}L^4)_6][SO_3CF_3]_8$ decayed rapidly out of solvent. Despite rapid handling and long exposure times, the data collected are less than ideal quality. Nevertheless, the data for the cages are of more than sufficient quality to unambiguously establish the connectivity of the structures. Reflecting the instability of the crystals, there is a large area of smeared electron density present in the lattice. Despite many attempts to model this region of disorder as a combination of solvent molecules and partial anions no reasonable fit could be found and accordingly this region was treated with the SQUEEZE function of PLATON. Table S2 lists the crystallographic parameters concerning data collection and structure refinements for the cages, while selected bond distances and angles are given in Table S3.

Table S3. Summary of crystallographic data for cages.

	Λ-[Ni$_4$(*R*-L^1)$_6$][ClO$_4$]$_8$	**Δ-[Ni$_4$(*S*-L^1)$_6$][ClO$_4$]$_8$**	**Δ-[Ni$_4$(*S*-L^2)$_6$][BF$_4$]$_8$**
formula	$C_{192}H_{240}Cl_4Ni_4N_{36}O_{16}$	$C_{192}H_{240}Cl_4Ni_4N_{36}O_{16}$	$C_{204}H_{264}B_6F_{24}N_{36}Ni_4O_{12}$
fw	3684.84	3684.84	4168.21
T (K)	173(2)	173(2)	173(2)
λ (Å)	0.71073	0.71073	0.71073
crystal system	Cubic	Cubic	Triclinic
space group	*I*23	*I*23	*P*1
a (Å)	23.432(2)	23.4359(5)	18.9274(16)
b (Å)	23.432(2)	23.4359(5)	19.8289(16)
c (Å)	23.432(2)	23.4359(5)	22.328(2)
α (^{0})	90	90	110.839(2)
β (^{0})	90	90	102.662(2)
γ (^{0})	90	90	108.564(2)
V (Å^3)	12866(2)	12872.0(5)	6881.8(10)
Z	2	2	1
D_{calc} (Mg/m^3)	0.951	0.951	1.006
μ (mm^{-1})	0.382	0.382	0.337
F(000)	3904	3904	2194
θ (^{0})	3.25- 25.02	3.25-25.29	3.07-23.66
index ranges	□16<=h<=27 □22<=k<=27 □22<=l<=27	□17<=h<=27 □27<=k<=22 □24<=l<=27	□21<=h<=20 □22<=k<=22 □25<=l<=25
reflections collected	11342	10160	48906
GOF (F^2)	1.343	1.131	1.038
R_1[a],wR_2[b](I>2σ(I))	0.1512, 0.3731	0.1120, 0.2942	0.0932, 0.1948
R_1[a],wR_2[b](all data)	0.1989, 0.3992	0.1623, 0.3282	0.1874, 0.2168

$R_1{}^a = \Sigma||F_o| - |F_c||/\Sigma F_o|$. $wR_2{}^b = [\Sigma w(F_o{}^2 - F_c{}^2)^2/\Sigma w(F_o{}^2)]^{1/2}$

	ΔΔΔΔ-[Ni$_4$(*S*-L^3)$_6$]Cl$_8$	**ΛΛΛΛ-[Ni$_4$(*R*-L^4)$_6$][SO$_3$CF$_3$]$_8$**
formula	$C_{240}H_{276}Cl_4Ni_4N_{36}O_6$	$C_{241}H_{264}Ni_4N_{36}O_3SF_3$
fw	4137.61	4036.78
T (K)	173(2)	173(2)
λ (Å)	0.71073	0.71073
crystal system	Cubic	Triclinic
space group	$F4_132$	$P1$
a (Å)	39.2624(10)	19.222(3)
b (Å)	39.2624(10)	20.854(3)
c (Å)	39.2624(10)	22.254(3)
α (^{0})	90	106.518(3)
β (^{0})	90	103.878(4)
γ (^{0})	90	112.172(3)
V (Å^3)	60524(3)	7289.2(17)
Z	8	1
D_{calc} (Mg/m^3)	0.908	0.920
μ (mm^{-1})	0.328	0.311
F(000)	17568	2141
θ (^{0})	3.07-25.24	3.01-19.25
index ranges	□34<=h<=47 □35<=k<=47 □46<=l<=24	□17<=h<=17 □19<=k<=19 □20<=l<=20
reflections collected	19996	33498
GOF (F^2)	1.126	1.015
R_1[a],wR_2[b](I>2σ(I))	0.0774, 0.1898	0.1010, 0.2209
R_1[a],wR_2[b](all data)	0.1229, 0.2048	0.1820, 0.2438

$R_1{}^a = \Sigma||F_o| - |F_c||/\Sigma F_o|$. $wR_2{}^b = [\Sigma w(F_o{}^2 - F_c{}^2)^2/\Sigma w(F_o{}^2)]^{1/2}$

Table S4. Selected bond lengths [Å] and angles [°] for cages.

		***ΛΛΛΛ*-[Ni$_4$(*R*-L^1)$_6$][ClO$_4$]$_8$**	
N(1)-Ni(1)	2.035(9)	N(3)-Ni(1)	2.096(9)
Ni(1)-N(1)#4	2.035(9)	Ni(1)-N(1)#5	2.035(9)
Ni(1)-N(3)#4	2.096(9)	Ni(1)-N(3)#5	2.096(9)
N(1)#4-Ni(1)-N(1)#5	93.1(3)	N(1)#4-Ni(1)-N(1)	93.1(3)
N(1)#5-Ni(1)-N(1)	93.1(3)	N(1)#4-Ni(1)-N(3)#4	78.7(4)
N(1)#5-Ni(1)-N(3)#4	91.4(4)	N(1)-Ni(1)-N(3)#4	170.8(4)
N(1)#4-Ni(1)-N(3)	91.4(4)	N(1)#5-Ni(1)-N(3)	170.8(4)
N(1)-Ni(1)-N(3)	78.7(4)	N(3)#4-Ni(1)-N(3)	97.3(3)
N(1)#4-Ni(1)-N(3)#5	170.8(4)	N(1)#5-Ni(1)-N(3)#5	78.7(4)
N(1)-Ni(1)-N(3)#5	91.4(4)	N(3)#4-Ni(1)-N(3)#5	97.3(3)
N(3)-Ni(1)-N(3)#5	97.3(3)		
		***ΔΔΔΔ*-[Ni$_4$(*S*-L^1)$_6$][ClO$_4$]$_8$**	
N(1)-Ni(1)	2.053(7)	N(3)-Ni(1)	2.123(7)
Ni(1)-N(1)#2	2.053(7)	Ni(1)-N(1)#3	2.053(7)
Ni(1)-N(3)#2	2.123(7)	Ni(1)-N(3)#3	2.123(7)
N(1)#2-Ni(1)-N(1)#3	92.9(3)	N(1)#2-Ni(1)-N(1)	92.9(3)
N(1)#3-Ni(1)-N(1)	92.9(3)	N(1)#2-Ni(1)-N(3)	91.6(3)
N(1)#3-Ni(1)-N(3)	170.9(3)	N(1)-Ni(1)-N(3)	79.0(2)
N(1)#2-Ni(1)-N(3)#2	79.0(2)	N(1)#3-Ni(1)-N(3)#2	91.6(3)
N(1)-Ni(1)-N(3)#2	170.9(3)	N(3)-Ni(1)-N(3)#2	97.0(2)
N(1)#2-Ni(1)-N(3)#3	170.9(3)	N(1)#3-Ni(1)-N(3)#3	79.0(2)
N(1)-Ni(1)-N(3)#3	91.6(3)	N(3)-Ni(1)-N(3)#3	97.0(2)
N(3)#2-Ni(1)-N(3)#3	97.0(2)		
		***ΔΔΔΔ*-[Ni$_4$(*S*-L^2)$_6$][BF$_4$]$_8$**	
N(1A)-Ni(1)	2.056(11)	N(3A)-Ni(1)	2.100(10)
N(1B)-Ni(2)	2.070(11)	N(1C)-Ni(1)	2.086(10)
N(1D)-Ni(3)	2.075(9)	N(1E)-Ni(1)	2.041(10)
N(3E)-Ni(1)	2.133(9)	N(1F)-Ni(4)	2.065(11)
N(3F)-Ni(4)	2.101(9)	N(1G)-Ni(2)	2.032(10)
N(3G)-Ni(2)	2.123(10)	N(1H)-Ni(3)	2.031(9)
N(1I)-Ni(2)	2.056(10)	N(1J)-Ni(4)	2.066(9)
N(3J)-Ni(4)	2.197(12)	N(1K)-Ni(3)	2.040(11)
N(1L)-Ni(4)	2.037(11)	N(3L)-Ni(4)	2.169(11)
Ni(1)-N(3C)	2.099(11)	Ni(2)-N(3I)	2.143(12)
Ni(2)-N(3B)	2.163(11)	Ni(3)-N(3D)	2.108(12)
Ni(3)-N(3H)	2.11(2)	Ni(3)-N(3K)	2.159(11)
Ni(3)-N(3S)	2.18(3)	N(1E)-Ni(1)-N(1A)	94.2(4)
N(1E)-Ni(1)-N(1C)	94.7(4)	N(1A)-Ni(1)-N(1C)	91.7(4)

N(1E)-Ni(1)-N(3C)	90.9(4)	N(1A)-Ni(1)-N(3C)	170.7(4)
N(1C)-Ni(1)-N(3C)	80.2(4)	N(1E)-Ni(1)-N(3A)	170.7(4)
N(1A)-Ni(1)-N(3A)	79.2(4)	N(1C)-Ni(1)-N(3A)	92.0(4)
N(3C)-Ni(1)-N(3A)	96.5(4)	N(1E)-Ni(1)-N(3E)	79.3(4)
N(1A)-Ni(1)-N(3E)	92.2(4)	N(1C)-Ni(1)-N(3E)	173.1(4)
N(3C)-Ni(1)-N(3E)	96.4(4)	N(3A)-Ni(1)-N(3E)	94.4(4)
N(1G)-Ni(2)-N(1I)	95.9(4)	N(1G)-Ni(2)-N(1B)	93.5(4)
N(1I)-Ni(2)-N(1B)	97.1(4)	N(1G)-Ni(2)-N(3G)	78.3(4)
N(1I)-Ni(2)-N(3G)	170.7(5)	N(1B)-Ni(2)-N(3G)	90.5(4)
N(1G)-Ni(2)-N(3I)	95.6(4)	N(1I)-Ni(2)-N(3I)	76.5(5)
N(1B)-Ni(2)-N(3I)	169.3(4)	N(3G)-Ni(2)-N(3I)	96.8(4)
N(1G)-Ni(2)-N(3B)	168.2(4)	N(1I)-Ni(2)-N(3B)	92.8(4)
N(1B)-Ni(2)-N(3B)	77.5(4)	N(3G)-Ni(2)-N(3B)	94.0(4)
N(3I)-Ni(2)-N(3B)	94.1(5)	N(1H)-Ni(3)-N(1K)	95.2(4)
N(1H)-Ni(3)-N(1D)	94.6(4)	N(1K)-Ni(3)-N(1D)	94.1(4)
N(1H)-Ni(3)-N(3D)	91.2(4)	N(1K)-Ni(3)-N(3D)	170.2(4)
N(1D)-Ni(3)-N(3D)	78.1(4)	N(1H)-Ni(3)-N(3H)	78.6(5)
N(1K)-Ni(3)-N(3H)	91.7(9)	N(1D)-Ni(3)-N(3H)	171.5(6)
N(3D)-Ni(3)-N(3H)	96.7(9)	N(1H)-Ni(3)-N(3K)	172.4(5)
N(1K)-Ni(3)-N(3K)	78.2(5)	N(1D)-Ni(3)-N(3K)	89.6(4)
N(3D)-Ni(3)-N(3K)	95.8(5)	N(3H)-Ni(3)-N(3K)	97.7(4)
N(1H)-Ni(3)-N(3S)	79.3(5)	N(1K)-Ni(3)-N(3S)	90.1(11)
N(1D)-Ni(3)-N(3S)	173.0(7)	N(3D)-Ni(3)-N(3S)	98.3(11)
N(3H)-Ni(3)-N(3S)	1.7(16)	N(3K)-Ni(3)-N(3S)	96.8(5)
N(1L)-Ni(4)-N(1F)	93.8(4)	N(1L)-Ni(4)-N(1J)	96.4(4)
N(1F)-Ni(4)-N(1J)	96.9(4)	N(1L)-Ni(4)-N(3F)	90.7(4)
N(1F)-Ni(4)-N(3F)	78.8(4)	N(1J)-Ni(4)-N(3F)	172.0(5)
N(1L)-Ni(4)-N(3L)	80.6(5)	N(1F)-Ni(4)-N(3L)	170.3(4)
N(1J)-Ni(4)-N(3L)	91.6(4)	N(3F)-Ni(4)-N(3L)	93.4(4)
N(1L)-Ni(4)-N(3J)	172.9(4)	N(1F)-Ni(4)-N(3J)	92.2(4)
N(1J)-Ni(4)-N(3J)	79.2(4)	N(3F)-Ni(4)-N(3J)	94.1(4)
N(3L)-Ni(4)-N(3J)	94.0(4)		
		***ΔΔΔΔ*-[Ni$_4$(*S*-L^3)$_6$]Cl$_8$**	
N(1)-Ni(1)	2.059(4)	N(3)-Ni(1)	2.172(4)
Ni(1)-N(1)#2	2.059(4)	Ni(1)-N(1)#3	2.059(4)
Ni(1)-N(3)#3	2.172(4)	Ni(1)-N(3)#2	2.172(4)
N(1)-Ni(1)-N(1)#2	92.05(14)	N(1)-Ni(1)-N(1)#3	92.05(14)
N(1)#2-Ni(1)-N(1)#3	92.05(14)	N(1)-Ni(1)-N(3)	79.16(17)
N(1)#2-Ni(1)-N(3)	170.54(17)	N(1)#3-Ni(1)-N(3)	91.75(16)
N(1)-Ni(1)-N(3)#3	170.54(17)	N(1)#2-Ni(1)-N(3)#3	91.75(16)

N(1)#3-Ni(1)-N(3)#3	79.16(17)	N(3)-Ni(1)-N(3)#3	97.47(15)
N(1)-Ni(1)-N(3)#2	91.75(16)	N(1)#2-Ni(1)-N(3)#2	79.16(17)
N(1)#3-Ni(1)-N(3)#2	170.54(17)	N(3)-Ni(1)-N(3)#2	97.47(15)
N(3)#3-Ni(1)-N(3)#2	97.47(15)		
	***ΛΛΛΛ*-[Ni$_4$(*R*-L^4)$_6$][SO$_3$CF$_3$]$_8$**		
N(1A)-Ni(1)	2.044(14)	N(1B)-Ni(2)	2.073(14)
N(1C)-Ni(1)	1.938(14)	N(1D)-Ni(3)	2.062(12)
N(1E)-Ni(1)	2.061(11)	N(1F)-Ni(4)	1.991(12)
N(1G)-Ni(2)	1.970(12)	N(1H)-Ni(3)	2.068(13)
N(1I)-Ni(2)	2.044(13)	N(1J)-Ni(4)	2.006(13)
N(1K)-Ni(3)	2.070(12)	N(1L)-Ni(4)	2.063(13)
N(3A)-Ni(1)	2.093(11)	N(3B)-Ni(2)	2.094(11)
N(3C)-Ni(1)	2.185(13)	N(3D)-Ni(3)	2.147(13)
N(3E)-Ni(1)	2.212(11)	N(3F)-Ni(4)	2.138(11)
N(3G)-Ni(2)	2.079(12)	N(3H)-Ni(3)	2.085(13)
N(3I)-Ni(2)	2.071(13)	N(3J)-Ni(4)	2.118(13)
N(3K)-Ni(3)	2.124(11)	N(3L)-Ni(4)	2.125(11)
N(1C)-Ni(1)-N(1A)	93.5(6)	N(1C)-Ni(1)-N(1E)	94.8(5)
N(1A)-Ni(1)-N(1E)	94.3(5)	N(1C)-Ni(1)-N(3A)	90.1(6)
N(1A)-Ni(1)-N(3A)	79.0(5)	N(1E)-Ni(1)-N(3A)	171.9(5)
N(1C)-Ni(1)-N(3C)	80.3(5)	N(1A)-Ni(1)-N(3C)	172.6(5)
N(1E)-Ni(1)-N(3C)	90.3(5)	N(3A)-Ni(1)-N(3C)	96.8(5)
N(1C)-Ni(1)-N(3E)	171.7(5)	N(1A)-Ni(1)-N(3E)	92.1(5)
N(1E)-Ni(1)-N(3E)	78.6(4)	N(3A)-Ni(1)-N(3E)	97.0(5)
N(3C)-Ni(1)-N(3E)	94.5(5)	N(1G)-Ni(2)-N(1I)	92.3(5)
N(1G)-Ni(2)-N(3I)	95.2(6)	N(1I)-Ni(2)-N(3I)	80.6(5)
N(1G)-Ni(2)-N(1B)	90.4(5)	N(1I)-Ni(2)-N(1B)	91.9(5)
N(3I)-Ni(2)-N(1B)	170.7(5)	N(1G)-Ni(2)-N(3G)	81.4(5)
N(1I)-Ni(2)-N(3G)	173.0(5)	N(3I)-Ni(2)-N(3G)	96.8(5)
N(1B)-Ni(2)-N(3G)	91.2(5)	N(1G)-Ni(2)-N(3B)	168.6(6)
N(1I)-Ni(2)-N(3B)	86.3(5)	N(3I)-Ni(2)-N(3B)	95.7(5)
N(1B)-Ni(2)-N(3B)	78.4(5)	N(3G)-Ni(2)-N(3B)	100.5(4)
N(1D)-Ni(3)-N(1H)	89.8(5)	N(1D)-Ni(3)-N(1K)	93.8(5)
N(1H)-Ni(3)-N(1K)	90.2(6)	N(1D)-Ni(3)-N(3H)	169.0(5)
N(1H)-Ni(3)-N(3H)	80.7(5)	N(1K)-Ni(3)-N(3H)	91.8(5)
N(1D)-Ni(3)-N(3K)	92.0(5)	N(1H)-Ni(3)-N(3K)	170.1(6)
N(1K)-Ni(3)-N(3K)	79.9(5)	N(3H)-Ni(3)-N(3K)	98.3(5)
N(1D)-Ni(3)-N(3D)	78.6(5)	N(1H)-Ni(3)-N(3D)	92.1(6)
N(1K)-Ni(3)-N(3D)	172.0(5)	N(3H)-Ni(3)-N(3D)	96.1(5)
N(3K)-Ni(3)-N(3D)	97.8(5)	N(1F)-Ni(4)-N(1J)	91.5(5)

N(1F)-Ni(4)-N(1L)	94.0(5)	N(1J)-Ni(4)-N(1L)	91.3(5)
N(1F)-Ni(4)-N(3J)	92.0(5)	N(1J)-Ni(4)-N(3J)	80.4(5)
N(1L)-Ni(4)-N(3J)	169.9(5)	N(1F)-Ni(4)-N(3L)	171.6(5)
N(1J)-Ni(4)-N(3L)	93.9(5)	N(1L)-Ni(4)-N(3L)	79.4(5)
N(3J)-Ni(4)-N(3L)	95.3(5)	N(1F)-Ni(4)-N(3F)	80.4(4)
N(1J)-Ni(4)-N(3F)	171.3(5)	N(1L)-Ni(4)-N(3F)	92.1(5)
N(3J)-Ni(4)-N(3F)	96.9(5)	N(3L)-Ni(4)-N(3F)	94.6(4)

For ***ΛΛΛΛ*-[Ni$_4$(*R*-L^1)$_6$][ClO$_4$]$_8$**: #1 x, -y+2, -z+2 #2 z, x, y #3 y, z, x #4 -y+1, z, -x+1 #5 -z+1, -x+1, y

For ***ΔΔΔΔ*-[Ni$_4$(*S*-L^1)$_6$][ClO$_4$]$_8$**: #1 -x+2, -y+2, z #2 y, z, x #3 z, x, y #4 -z+1, -x+1, y #5 -y+1, z, -x+1

For ***ΔΔΔΔ*-[Ni$_4$(*S*-L^3)$_6$]Cl$_8$**: #1 -x+1/2, -y+1/2, z+0 #2 -y+1/2, z+0, -x+1/2 #3 -z+1/2, -x+1/2, y+0

15. References

[1] F. L. Zhang, J. Q. Chen, L. F. Qin, L. Tian, Z. Li, X. Ren, Z. G. Gu, 2016, *Chem. Commun.,* **52**, 4796-4799.

[2] A. Wolfe, G. H. Shimer Jr, T. Meehan, *Biochemistry*, 1987, **26**, 6392–6396.

[3] I. Haq, P. Lincoln, D. Suh, B. Norden, B. Z. Chowdhry, J. B. Chaires, 1995, *J. Am. Chem. Soc.,* **117**, 4788-4796.

[4] *SAINT-Plus*, version 6.02; Bruker Analytical X-ray System: Madison, WI, 1999.

[5] G. M. Sheldrick, *SADABS An empirical absorption correction program*; Bruker Analytical X-ray Systems: Madison, WI, 1996.

[6] G. M. Sheldrick, *SHELXTL-97*; Universität of Göttingen: Göttingen, Germany, 1997.